Review

A Review of Hydrogen Direct Injection for Internal Combustion Engines: Towards Carbon-Free Combustion

Ho Lung Yip [1] , **Aleš Srna [1]** , **Anthony Chun Yin Yuen [1]** , **Sanghoon Kook [1]** , **Robert A. Taylor [1,2]** , **Guan Heng Yeoh [1]** , **Paul R. Medwell [3]** and **Qing Nian Chan [1,*]**

[1] School of Mechanical and Manufacturing Engineering, University of New South Wales, Sydney 2052, Australia; h.l.yip@unsw.edu.au (H.L.Y.); a.srna@unsw.edu.au (A.S.); c.y.yuen@unsw.edu.au (A.C.Y.Y.); s.kook@unsw.edu.au (S.K.); robert.taylor@unsw.edu.au (R.A.T.); g.yeoh@unsw.edu.au (G.H.Y.)

[2] School of Photovoltaic and Renewable Energy Engineering, University of New South Wales, Sydney 2052, Australia

[3] School of Mechanical Engineering, The University of Adelaide, Adelaide 5005, Australia; paul.medwell@adelaide.edu.au

* Correspondence: qing.chan@unsw.edu.au

check for updates

Abstract: A paradigm shift towards the utilization of carbon-neutral and low emission fuels is necessary in the internal combustion engine industry to fulfil the carbon emission goals and future legislation requirements in many countries. Hydrogen as an energy carrier and main fuel is a promising option due to its carbon-free content, wide flammability limits and fast flame speeds. For spark-ignited internal combustion engines, utilizing hydrogen direct injection has been proven to achieve high engine power output and efficiency with low emissions. This review provides an overview of the current development and understanding of hydrogen use in internal combustion engines that are usually spark ignited, under various engine operation modes and strategies. This paper then proceeds to outline the gaps in current knowledge, along with better potential strategies and technologies that could be adopted for hydrogen direct injection in the context of compression-ignition engine applications—topics that have not yet been extensively explored to date with hydrogen but have shown advantages with compressed natural gas.

Contents

1. Introduction

Constrained carbon-emission budgets and increasingly stringent emission standards for vehicles around the globe have placed enormous pressure on manufacturers to develop less carbon-intensive fleets. Despite the present global domination of internal combustion engine (ICE) in the transportation section, a number of legislative strategies have been developed and adopted to promote a gradual replacement of ICE propulsion technology by fuel cell (FC) and battery-electric vehicles [1], unless there is a breakthrough in ICE technology to enable a significant reduction of harmful emissions and dependence on fossil fuel. Hydrogen has long been considered a future fuel in transportation powertrains, due to its ability to eliminate carbon-based emissions (e.g., CO, CO_2 and soot) and to achieve high energy efficiency [2]. Furthermore, hydrogen can be produced from renewable energy sources [3]. The first reported successful commercial application of hydrogen-powered vehicles dates back to the 1930s, with more than 1000 vehicles converted into hydrogen and flexible hydrogen/gasoline operation; however, technical details were reportedly destroyed because of war and can no longer be found [4]. The development of hydrogen-fueled ICEs stagnated since, with ongoing scientific research but limited practical applications. During the second half of the 20th century, hydrogen-fueled ICEs were mainly demonstration projects. Recently, effort towards decarbonization and tightening emission standards has facilitated several breakthroughs in the development of renewable hydrogen technologies, including: advanced methods and materials for hydrogen storage (e.g., high pressure storage, up to 700 bar), production (e.g., solar thermo-chemical processes) and usage (e.g., high pressure direct in-cylinder injection of gas). These developments have catalyzed the re-ignition of global interests towards incorporating hydrogen as an energy carrier in powertrains [5,6]. The Hydrogen Council, a global initiative for hydrogen energy composed of various energy and transportation companies, estimated that approximately 25% of the passenger vehicles and 20% of the non-electrified rail transport would be fueled with hydrogen by 2050, potentially reducing daily oil consumption for transportation use by up to 20% [7,8].

1.1. Hydrogen Application and Production

In the hydrogen economy—a future scenario where hydrogen represents the primary energy carrier—hydrogen has a wide range of applications other than transportation. For instance, many industrial processes require high-grade heat, which can utilize hydrogen combustion as a more efficient route [7]. Hydrogen is also an important reactant in the production of industrial feedstocks such as ammonia, methanol, polymers as well as in other refining processes, including fuel desulfurization, iron making and conversion of captured CO_2 from air or flue gas into useful chemicals [7]. Countries including the United Kingdom (UK), the United States (US), South Korea and some

European countries have developed infrastructure to use natural gas as power and heating sources in buildings. Such infrastructure brings additional benefit from a convenient switch to hydrogen-methane blend for further decarbonization [7]; nevertheless, a technology advancement is required to facilitate the increased share of hydrogen. The universal applicability of hydrogen for modern energy needs has boosted the investment and development of renewable hydrogen production and its related technology by many countries, with China being the largest importer and the US being the largest exporter, as of 2017 [9]. Australia [10,11], Japan [12] and Germany [13] have also devised strategic plans to become major players in the potential future hydrogen economy.

As of 2016, 96% of the total hydrogen production (i.e., ∼55 million tonnes per annum [7]) originated from fossil fuels [14]. Apart from the thermo-chemical conversion of coal and oil into hydrogen, steam methane reforming is the most widely adopted method for hydrogen production due to its cost effectiveness [15]. This is achieved by the chemical reaction between purified methane or natural gas and high temperature (i.e., 970–1120 K) and pressure (i.e., 3–25 bar) steam in the presence of a catalyst, which is typically nickel [6]. It should be noted that CO_2 is produced during the steam methane reforming process. Therefore, and due to the fossil feedstock, hydrogen produced through these chemical pathways is not considered renewable.

On the other hand, electrolysis of water, an electro-chemical process of splitting water into oxygen and hydrogen using electric current, can be considered renewable if the electricity is sourced renewably, such as using hydro, wind or solar power. This method currently accounts for only 4% of the world hydrogen production but it is predicted to expand rapidly to 22% by 2050 [16]. The research community has also been developing other renewable hydrogen production pathways, including photocatalytic hydrogen production, biomass and waste gasification and biological hydrogen production through biomass fermentation, etc. Some of these technologies are expected to mature and to enter commercial scale production by 2030 [17] and will boost the production of hydrogen through renewable routes. Therefore, green hydrogen will become more readily available and find widespread application in energy generation systems and powertrains.

1.2. The Potential for Hydrogen

With abundant land and renewable energy resources, a number of countries are advantageously poised to produce green hydrogen at low cost and to implement a hydrogen economy for domestic use or export to their neighbouring countries with high energy demands. This is because, unlike electricity, hydrogen can be stored and transported over long distances at lower cost. In particular for countries such as Australia and Chile, their geographic locations and well-established reputation as reliable conventional energy exporters could make them major hydrogen suppliers targeting their neighbours with net demands, such as China, Japan and Korea [18]. In fact, such collaboration is already underway with a joint project between Australia and Kawasaki Heavy Industries (Japan) to build a hydrogen supply chain between the two countries, wherein Japan is forecasted to import 900,000 tons of hydrogen by 2030 [19]. This strategic hydrogen export opportunity is estimated to add as much as AUD10 billion to Australia's economy by 2040 in a high hydrogen demand scenario [19]. European countries with a considerable production of renewable electricity, as well as mature infrastructure and transportation facilities for natural gas, such as the Netherlands, are also poised to benefit from an increased use of hydrogen energy [20]. The potentials to store excess electricity in the form of hydrogen and to adopt existing gas pipelines for hydrogen transportation as the production volume increases, place the Netherlands in an advantageous position as an energy exporter. The attractiveness is demonstrated by an estimated ∼EUR17.5–25 billion investment by 2025 to develop a carbon-free hydrogen economy in the Northern Netherlands [20].

These figures may have a significant growth potential, considering that industrial applications, for instance oil refining (33%), ammonia production (27%), methanol production (11%) and steel production (3%) currently dominates the use of hydrogen and drives more than 50% of the demand; while the use of hydrogen for power generation and propulsion only accounts for 1–2% of the total

consumption [19,21]. For the transportation sector, the low utilization could be attributed to the lack of hydrogen distribution infrastructure and the slow development of hydrogen powertrain that can efficiently and cost-effectively convert hydrogen into power. There is, therefore, significant room for growth for increased hydrogen usage in the transportation sector, as technologies surrounding hydrogen transportation and usage continue to improve and mature.

1.3. Recent Developments of Hydrogen Applications in the Transportation Sector

Hydrogen powertrains mainly utilize two energy conversion technologies—hydrogen FC and ICE. An FC, which converts hydrogen into electrical energy used for propulsion, is presently the more commercialized approach. A FC vehicle is reported to have a tank-to-wheel efficiency in the range from 31% to 36%, with water vapor being the only emission [22,23]. Toyota, Honda and Hyundai have already commercialized FC vehicles in selected markets, with more than 6500 units sold as of June 2018 [24]. A prototype FC truck with a range of 480 km was recently unveiled by Toyota and Kenworth [25], demonstrating the potential to replace the ICE technology in future heavy-duty applications.

The advantages of hydrogen ICE compared to the FC technology include a higher tolerance to fuel impurities, flexibility to switch between fuels, reduction of rare materials usage and a more straightforward transition from conventional vehicles [26]. In addition, hydrogen ICE technology benefits from the reduced cost of using the existing mature manufacturing facilities and processes for conventional ICEs. The development of advanced hydrogen ICEs (e.g., direct injection (DI) and dual-fuel methods) is still in the conceptual stage. A majority of hydrogen-fueled ICE prototypes use port fuel injection (PFI) system, benefiting from a straightforward conversion from existing gasoline engines. A proof-of-concept light-duty truck and 'microbus' powered by such hydrogen-fueled ICE was presented by Tokyo City University [26]. It has to be noted that even with such a simple modification, engine brake thermal efficiency (BTE) of ~30–37% at medium load was reported [27], readily comparable with the current FC technology. Despite the competitive peak efficiency, hydrogen PFI suffers from a series of issues that will be discussed in Section 4, which can be tackled by an advanced DI fuel system as further discussed later in Sections 5 and 6. The potential of DI system has been already demonstrated by BMW and its partners in 2009. A hydrogen DI system with up to 300 bar injection pressure has been developed and integrated into a spark-ignition (SI) engine, achieving a maximum efficiency of 42%, paralleling diesel engines with turbocharging [28]. In light of the potential of hydrogen engine, Mazda has been developing a hydrogen rotary engine combining PFI and DI technology since 2006. This technology has been integrated into a sports-car model with an extended driving range of 649 km [29]. Furthermore, a series of works on experimental metal and optical engines as well as numerical simulations for hydrogen DI was funded by the U.S. Department of Energy from 2004 to 2011 [30–39]. A peak BTE of 45% in a hydrogen ICE was demonstrated at 2000 rpm and a high load condition of 13.5 bar brake mean effective pressure (BMEP). Most recently, the Australian Renewable Energy Agency (ARENA) has allocated more than AUD22 million to develop an effective renewable energy supply chain centered around hydrogen, including an investment in developing advanced hydrogen ICE technology and support for establishing a fundamental understanding of hydrogen combustion in engines [10].

1.4. Scope

The potential of more readily available renewable hydrogen is often associated with its potential to reduce the consumption of fossil fuels and harmful combustion emissions, when used in energy generation. While technologies for producing and storing hydrogen are under development, current bottleneck to efficiently utilize hydrogen needs to be overcome especially in the transportation section, as a large contributor to carbon emissions. Thus, this paper reviews the current development of using hydrogen in the transportation sector, with a focus on hydrogen combustion in ICEs. The properties of hydrogen and their implications on the use in ICEs will first be discussed in Section 2. Different

injection and ignition methods will be compared from Sections 4 and 5 in terms of performance and emissions, with a focus on hydrogen DI. A novel ignition strategy utilizing a small amount of pilot diesel jet to auto-ignite the hydrogen DI jet is proposed and evaluated in Section 6 as a solution to current issues associated with hydrogen DI. This is also known as the dual-fuel hydrogen-diesel direct injection (H2DDI) mode. Due to the need of in-depth understanding of the underlying combustion mechanisms in this proposed combustion mode, studies of the behaviour of high pressure hydrogen jets will be reviewed to map out the current level of fundamental understanding in Section 7. It is followed by a review of available hydrogen DI hardware as well as hydrogen DI injector design considerations in Section 8, which are required to facilitate development in this field. Discussion of the necessary next steps for hydrogen ICE will be provided by reviewing and evaluating this information.

2. Hydrogen Properties and Their Implications on Use in Internal Combustion Engine

Hydrogen has unique physical and chemical properties, compared to the conventional fossil fuels widely used in the transportation sector, namely compressed natural gas (CNG), gasoline and diesel, as shown in Table 1 [4,27,40–42]. Engine performance with these fuels in different engine modes is commonly compared with hydrogen and will be discussed throughout the study. One of the many advantages of using hydrogen in ICE as a clean alternative fuel is its zero carbon content. This means that carbon-based emissions, mainly CO, CO_2 and soot, can be eliminated, leaving NO_x as the only harmful combustion byproduct. With a high specific energy density, hydrogen can provide nearly three times as much energy by mass compared with other fossil fuels, reflected in its lower heating value.

Table 1. Hydrogen properties compared with compressed natural gas (CNG), gasoline and diesel.

Property	Hydrogen	CNG	Gasoline	Diesel
Carbon content (mass%)	**0**	75 [e]	84	86
Lower heating value (MJ/kg)	**119.7**	45.8	44.8	42.5
Density [a,b] (kg/m^3)	**0.089**	0.72	730–780	830
Volumetric energy content [a,b] (MJ/m^3)	**10.7**	33.0	33×10^3	35×10^3
Molecular weight	2.016	16.043 [e]	$\sim$110	$\sim$170
Boiling point [a] (K)	20	111 [e]	298–488	453–633
Auto-ignition temperature (K)	**858**	813 [e]	$\sim$623	$\sim$523
Minimum ignition energy in air [a,d] (mJ)	**0.02**	0.29	0.24	0.24
Stoichiometric air/fuel mass ratio	34.5	17.2 [e]	14.7	14.5
Stoichiometric volume fraction in air (%)	29.53	9.48	$\sim$2 [f]	-
Quenching distance [a,c,d] (mm)	**0.64**	2.1 [e]	$\sim$2	-
Laminar flame speed in air [a,c,d] (m/s)	**1.85**	0.38	0.37–0.43	0.37–0.43 [g]
Diffusion coefficient in air [a,b] (m^2/s)	8.5×10^{-6}	1.9×10^{-6}	-	-
Flammability limits in air (vol%)	4–76	5.3–15	1–7.6	0.6–5.5
Adiabatic flame temperature [a,c,d] (K)	2480	2214	2580	$\sim$2300

[a] at 1 bar, [b] at 273 K, [c] at 298 K, [d] at stoichiometry, [e] methane, [f] vapor and [g] n-heptane.

There are, nonetheless, a number of drawbacks related to the very low density of hydrogen (i.e., low volumetric energy content (MJ/m^3)). At atmospheric pressure and 273 K, the density of hydrogen is an order of magnitude less than that of natural gas, due to the very low molecular weight of hydrogen. The low boiling point suggests that compressed hydrogen will be the most prominent storage option. This presents a significant challenge for the implementation of hydrogen ICE in on-road applications due to the limited vehicle space. Increasing storage pressure is required to increase hydrogen density and hence the volumetric energy content. For instance, hydrogen at 350 bar (i.e., a current standard supply pressure for hydrogen refuelling) and 273 K can increase the gas density to $\sim$31 kg/m^3 or the volumetric energy content to $\sim$3700 MJ/m^3.

With the highest auto-ignition temperature and Research Octane Number (RON $\geq$ 130) [43] relative to the common fuels, the resistance of hydrogen to knocking is expected to be high. However, its minimum ignition energy in air at stoichiometry is an order of magnitude less than that of hydrocarbon

fuels, which indicates that hydrogen can be easily ignited by hot spots or residues in combustion chamber. This may lead to pre-ignition of fuel, which is characterized by combustion during the compression stroke prior to the intended ignition. This results in a loss of combustion phasing control, knocking and possibly mechanical engine failure. It should be noted that the global effect of pre-ignition and knock is nearly indistinguishable [27], since pre-ignition usually leads to knock. However, the underlying causes for the two phenomena are very different. A previous study [44] has shown that the Motor Octane Number (MON) of hydrogen is much less than its RON, compared to the typical 8–10 points decrease for the gasoline fuel; although the exact value of hydrogen MON was not clear. Nevertheless, MON is reported to be a more accurate knock resistance metric in hydrogen engine designs [43]. This explains the frequent report of knock in hydrogen engine applications.

The quenching distance of hydrogen is small compared to conventional hydrocarbon fuels. Consequently, higher temperature gradients near the combustion chamber walls can be expected, leading to increased combustion heat losses. When hydrogen is used in PFI engine applications, the short quenching distance along with the high laminar flame speed in air imply an increased propensity for flame backfiring into the intake manifold. This issue can be alleviated by modifying engine geometry, reducing the crevice volume, retuning of engine operating conditions and a complete removal of abnormal discharge and residual electric energy in the ignition system [45,46]. Also, a non-platinum cold-rated spark plug should be used to avoid pre-ignition and backfiring in SI engine [47]. This is because the platinum material in the spark plug can result in an undesired catalytic response with hydrogen and air. A cold-rated spark plug, on the other hand, can facilitate quick heat transfer to minimize hydrogen exposure to hot spots that may lead to engine knock and abnormal combustion. This is where hydrogen DI shows a great advantage as the backfiring can be completely avoided using the injection after the intake valve closing.

Nevertheless, the unique physical and thermo-chemical properties of hydrogen can facilitate the design of a highly efficient ICE. For instance, the dispersion of hydrogen is four times faster than that of CNG, which can be inferred by comparing their diffusion coefficients in air in Table 1. This can promote in-cylinder fuel and air mixing in ICEs. The stoichiometric hydrogen volume fraction corresponds to 29.53 vol%. Nevertheless, the wide flammability limit from 4–76 vol% hydrogen in air, alongside with the high flame speed, indicates that hydrogen ICE can operate considerably lean, thus improving thermal efficiency. The adiabatic flame temperature of hydrogen at stoichiometry is relatively high, which promotes NO_x formation. However, lean operations or a high level of exhaust gas recirculation (EGR) can be used to reduce NO_x emissions due to the wide flammability limits.

It should be noted that utilizing hydrogen in ICEs may induce other safety concerns related to the on-board fuel storage and delivery system. For example, hydrogen embrittlement is a common cause of material failure when high pressure hydrogen is used [48]. Also, the high diffusivity of hydrogen indicates that hydrogen poses a high risk of leakage. These issues require special measures in the design of the vehicle and the fuel delivery system but are not the main focus of this study. Moreover, these challenges are commonly shared with the FC option for powering vehicles.

3. Hydrogen Engine Combustion Modes

A general categorization of hydrogen ICE technology is presented in Figure 1. Broadly, engines can be divided into two main categories based on the fuel injection method—PFI and DI. The ignition methods of hydrogen PFI engines typically employ spark discharge, dual-fuel operation with pilot diesel DI or auto-ignition in the homogeneous charge compression ignition (HCCI) mode. The hydrogen DI studies commonly employ spark-assisted or hot-surface-assisted (i.e., glow plug) ignition. This injection mode also possesses the potential to employ dual-fuel mode, with hydrogen ignited by a high temperature environment created by the pilot diesel-fuel combustion, known as the H2DDI mode. This injection strategy has, however, been more frequently studied with CNG instead of hydrogen, as discussed later in Section 6.
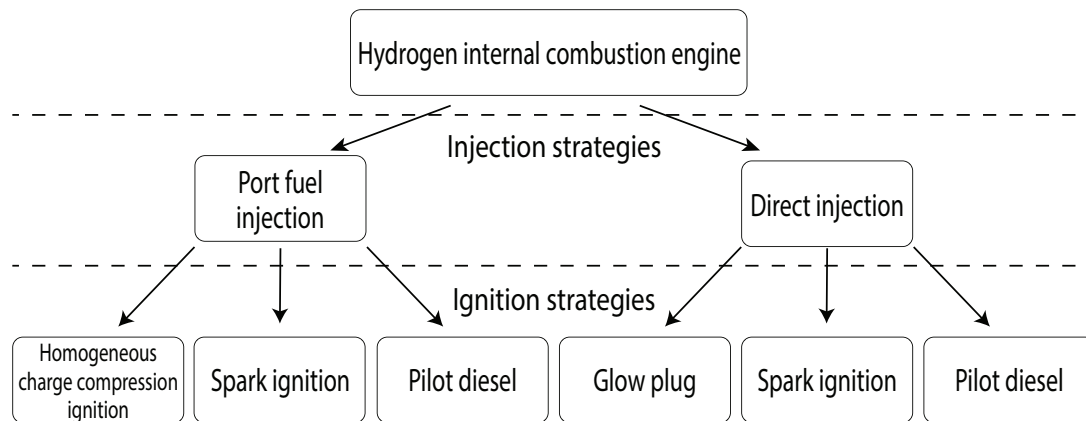
Figure 1. Categorization of hydrogen internal combustion engine (ICE) based on typical injection and ignition strategies.

4. Hydrogen Port Fuel Injection

PFI is a widespread fuel delivery strategy for SI ICEs—fuel is injected during the intake stroke into the intake port upstream of the intake valve. The modification of conventional PFI ICE to hydrogen involves a comparatively straightforward replacement of the injection system. However, as mentioned previously, this engine combustion mode operated with hydrogen fuel can suffer from a number of issues, such as pre-ignition, knock and backfiring due to the low minimum ignition energy and quenching distance of hydrogen. On the other hand, hydrogen displaces air in the intake and therefore limits engine power density. PFI also increases the work needed during the compression stroke compared with late hydrogen DI. These factors often lead to reduced power output and deteriorated efficiency of engines with hydrogen PFI. Combustion characteristics and engine performance of hydrogen PFI engines with different ignition strategies are discussed below.

4.1. Homogeneous Charge Compression Ignition

Due to the high diffusion coefficient of hydrogen, a homogeneous hydrogen-air mixture can be formed more readily than with other conventional fuels. HCCI mode with hydrogen fuel can be operated under very fuel-lean conditions, reducing NO_x formation while maintaining high engine efficiency [49]. Caton and Pruitt [50] found that NO_x emissions of hydrogen HCCI are nearly zero (i.e., ~1 ppm) and are one to three orders of magnitude less than that of conventional diesel operation at low load, compression ratio of 18 and intake temperature of 373 K. Nevertheless, the applicability of this combustion mode is limited by the high auto-ignition temperature of hydrogen—an unrealistic compression ratio of 42 would be required for HCCI combustion at equivalence ratio (ϕ) of 0.1, room temperature and cold start in a 0.5 L single-cylinder compression-ignition (CI) engine [51]. Control of the combustion phasing and peak pressure rise rate are some other challenges—high rate of heat release is commonly reported [51,52], which affects engine reliability. A previous study [53] in a 1.6 L single-cylinder CI engine reported that 10–90% of the total heat release occurs within ~3° crank angle (CA) at 1200 rpm, compression ratio of 17, ϕ of 0.2 and intake temperature of 390 K. Although a high engine indicated thermal efficiency (ITE) of 45% can be achieved with hydrogen HCCI, the achievable load was found to be limited at 3 bar indicated mean effective pressure (IMEP), which is half of the load limit in hydrogen SI PFI operation and 25% of the load limit in gasoline SI operation [53]. Increasing the engine load (i.e., rising ϕ) also causes higher NO_x emissions, due to advanced combustion phasing and thus increased peak temperature [50].

4.2. Spark-Ignited Port Fuel Injection

Hydrogen PFI SI engine is one of the most investigated modes of hydrogen ICE. The performance and control strategies of this engine mode have been reviewed in depth by Das [4] and White et al. [27].

In summary, running the engine at ultra-lean conditions (i.e., $\phi \leq 0.5$) can lower NO_x emissions to below 100 ppm without aftertreatment. Under stoichiometric condition using EGR and a three-way catalytic converter, a near zero engine-out NO_x emissions (i.e., less than 1 ppm) has been demonstrated [54,55]. Knocking, pre-ignition and backfiring are some of the well identified problems in this combustion mode [56], limiting the engine power output by forcing a very lean operation. Previous studies [27,57] have shown that the minimum ignition energy of hydrogen-air mixtures at atmospheric pressure increases exponentially with a decreasing ϕ from stoichiometry, which can alleviate the pre-ignition problem. The exact ϕ limit for engine operation depends on compression ratio, mixture temperature and engine speed, and so forth. Typically, the peak power output of hydrogen PFI SI engine decreases between 35% and 50%, compared to gasoline operation [58,59]. Despite the penalty in engine power, lean operation contributes to reduced combustion heat losses and increases the charge specific heat ratio, therefore improving engine BTE. A peak engine BTE of 38% at optimized compression ratio of 14.5 and $\phi = 0.55$ has been reported for a 2-L four-cylinder engine [58]. Nevertheless, the on-going development of more advanced engine technologies, for instance turbocharging with intake charge cooling and hydrogen DI, has the potential to alleviate the drawbacks of hydrogen PFI SI engine and even to improve engine BTE, as discussed later in Sections 5 and 6.

4.3. Pilot-Fuel-Ignited Engine with Port Hydrogen Injection

Ignition of a port-injected hydrogen charge can be triggered by a DI of pilot diesel fuel, as commonly employed in converted CI engines. One of the main advantages of this mode is its flexibility of hydrogen share in the total energy input. Usually, the substitution rate of diesel fuel with hydrogen is limited by the excessive rate of pressure rise and end-gas knocking of the well premixed charge. Also, at high hydrogen energy ratio, the increased ϕ raises the tendency for pre-ignition, similar to SI engine applications. As reviewed elsewhere, a majority of previous investigations were limited to a hydrogen energy share of ~30–40% at low and medium loads and ~6–25% at high load [60,61]. While a study by Santoso et al. [62] demonstrated a utilization of 97% hydrogen energy share in this engine mode is possible in a single-cylinder compression-ignition engine at 1.9 bar BMEP, a trade-off in the engine efficiency was also reported with increased hydrogen share. In terms of pollutant emissions, most studies show that this working mode cannot significantly alleviate the emissions of CO and particulate matter, while the emissions of CO_2 in first order decrease proportionally to the energy substitution rate. Nevertheless, over 50% of CO and smoke emission reduction relative to diesel operation has been reported at substitution rate of 46% [63]. The effect of diesel substitution with hydrogen on NO_x emissions is still not fully understood and contradictory engine testing results were reported [60]. For instance, Saravanan et al. [64] claimed that NO_x emissions can be lowered if hydrogen substitution is more than 30% of energy share, which was attributed to a reduced peak combustion temperature. To the contrary, Sandalci et al. [63] reported that increased NO_x emissions with hydrogen addition under all tested conditions, from 0–46% hydrogen energy fraction. This was attributed to the pathway of unburned hydrogen, oxidized to HO_2, boosting the conversion of NO to NO_2 [60]. This shows that the underlying mechanisms, governing the efficiency and pollutant formation in this combustion mode, are still not well understood. Undoubtedly, in the current state of technology, this combustion mode cannot fulfill the future emission legislation. The potential for the substitution of conventional fuel is also limited. Different injection strategies and charge cooling strategies should be further developed to improve NO_x emissions and pre-ignition problem leading to a higher hydrogen share, respectively, for this engine mode [60]. While hydrogen PFI is relatively straightforward to implement with the current engine technology and can be used in short term to promote hydrogen ICE development, more advanced combustion strategies are required to overcome the limitations of PFI in achieving high engine loads and reducing emissions.

5. Hydrogen Only Combustion with Direct Injection

A promising approach to improve hydrogen engine performance is to inject hydrogen directly into the cylinder during the compression stroke [65]. By doing so, the backfiring problem of PFI configuration can be avoided, since fuel injection occurs when the intake valves are already completely closed. Pre-ignition issue can also be avoided to a certain extent by reducing the exposure time of hydrogen mixture to hot-spots. The volumetric efficiency loss for PFI due to the displacement of air by hydrogen, as discussed above, is no longer an issue, if injection occurs after the inlet valves are closed. When injecting fuel late during the compression stroke, high injection pressure (i.e., ≥ 100 bar) is required to overcome the elevated in-cylinder pressure. Concurrently, higher injection pressure can increase fuel mass flow rate compared to typical low pressure PFI, which can provide higher energy input for the same injection duration, to drive high load operation. Therefore, a number of studies [38,65,66] demonstrated that high load hydrogen high pressure direct injection (HPDI) operation, under optimal operating conditions, can achieve similar efficiency as traditional diesel engines. Hydrogen HPDI also enables very flexible engine operation due to the many tuning parameters, for instance injection pressure, injection duration, ignition timing and injector orientation, which can be tuned to optimize the engine performance.

However, the high auto-ignition temperature of hydrogen still has to be overcome. Aleiferis and Rosati [43] investigated hydrogen DI HCCI mode in an optical engine with a compression ratio of 7.5 and it was reported that air intake preheating and high non-cooled internal EGR level are needed to auto-ignite hydrogen in this mode. It should be noted the mixture homogeneity may be affected by the late hydrogen DI after the intake valve is closed. Single-kernel flame propagation was also observed from OH laser induced fluorescence results for all equivalence ratios studied from 0.40 to 0.59, which is atypical to the multi-kernel fast combustion for hydrocarbon fuels in HCCI [43]. Authors proposed that coupling SI after the start of auto-ignition can establish a second flame front expanding towards the first one, similar to twin-spark engines, for better controlled auto-ignition. Glow plug and diesel pilot are also common ignition sources reported in literature. It is noted that hydrogen HPDI has been applied in modified SI as well as CI engines with a range of compression ratios. Typically, the conventional fuel injection system was replaced by a high pressure injection system for hydrogen DI. Additional engine modifications are required to accommodate the ignition assistance of choice.

5.1. Glow-Plug-Assisted Ignition

A glow plug is a device featuring an electrically heated surface protruding into the engine combustion chamber. It is a common equipment in diesel engines to assist engine cold start by increasing local charge temperature. When used in hydrogen DI ICE as conceptualized in Figure 2, the glow plugs need to operate continuously to ensure hydrogen ignition in every engine cycle. The required glow-plug's surface temperature in the range from 1200 to 1400 K was reported [67–69]. In 1979, Homan et al. [67] reported that glow plug is a more reliable ignition source for hydrogen ignition—a short and stable delay between the start of injection (SOI) and ignition of 10°–13° CA in a cooperative fuel research engine at 1240 rpm and compression ratio of 18 was reported. This ignition performance was compared to a multi-strike spark-plug ignition system (2.5 kHz strike rate), where a fluctuating delay of 0–25° CA between the injection and the initial pressure rise was observed. Homan et al. [67] attributed this fluctuation to a smaller surface area of the spark gap relative to the glow plug. A previous study [70] has shown that the glow-plug ignition method suffers from ~10% increased specific fuel consumption relative to diesel operation—for instance, at 5 bar IMEP and 1200 rpm the ITE decreased from approximately 47% to 42%. Although NO_x emissions in this combustion mode were lower than that in diesel operation, it was still significant, especially at high load (i.e., >500 ppm) [70]. Nevertheless, the above findings were from early research conducted decades ago. The durability of the glow plug due to the high surface temperature is questionable when it comes to commercial application and thus this technology is rarely used in recent engine development [71].
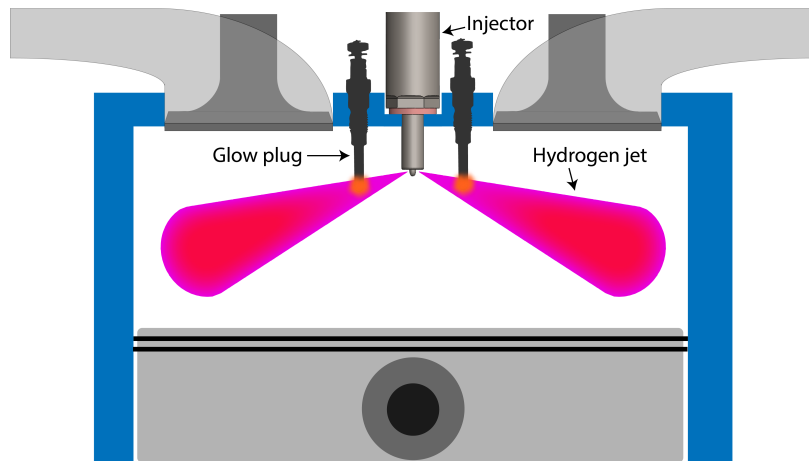
Figure 2. Schematic of the glow plug assisted ignition of hydrogen direct injection.

5.2. Spark-Assisted Ignition

A wealth of spark-assisted hydrogen DI combustion engine studies is available in literature, making this combustion concept the most investigated approach for hydrogen DI. The progress of hydrogen spark-assisted-ignition engines up to year 2013 was reviewed by Verhelst [26] and thus only some highlights and recent development are included in this review. The most common engine configuration is very similar to that of glow-plug-assisted ignition shown in Figure 2, with the glow plugs replaced by one or more spark plugs. In many research studies, the injector and spark plug arrangement was confined by the geometry of production cylinder head used for modification.

Wimmer et al. [40] converted a single-cylinder automotive size SI engine into hydrogen DI engine and achieved an ITE of 40% at low and medium loads, only slightly inferior to the state-of-art light-duty diesel engine at that time. A significant conclusion was that injection timing directly affects mixture homogeneity, which more significantly influences engine performance and emissions than ignition timing. Retarding SOI timing, from 120° to less than 65° CA before top dead center (BTDC), was found to improve overall engine efficiency. This is attributed to the more stratified mixture, which results in a faster initial flame development and improved combustion phasing, despite the increased local wall heat flux caused by the fuel-rich zone near spark plug and short hydrogen quenching distance. Furthermore, compression work during the compression stroke can be reduced as well since hydrogen is injected into an already compressed charge. The influence of injection timing on NO_x emissions is engine load dependent—at medium and low loads, NO_x emissions increase with delayed injection timing, attributed to a less homogeneous mixture leading to diffusion combustion and the formation of lean and hot zones. To the contrary, at high loads, NO_x emissions increase significantly for early injection, attributed to the global equivalence ratio becoming favorable for NO_x production. The effect of EGR on the NO_x emissions has also been investigated and a trade-off of efficiency was reported similar to the results from studies using hydrogen PFI. The validity of injection timing effects on the efficiency and NO_x emissions at low and medium load in SI DI engines by Wimmer et al. [40] has been confirmed by Kawamura et al. [72], Tanno et al. [73] and Takagi et al. [74], despite differences in engine geometry and operating condition (e.g., engine displacement, compression ratio, injection pressure, injection timing). In addition, under the low and medium loads, increasing the injection pressure can reduce NO_x emissions by promoting air entrainment and mixing [73,74] but at a cost of lower efficiency due to the increased engine wall heat losses associated with increased wall impingement arising from the longer jet penetration [73]. A more recent study by Takagi et al. [75] indicated that the injection angle has a strong impact on engine performance and needs to be optimized in order to reduce wall heat loss by ensuring best separation of the hydrogen jets from the chamber walls.

The hydrogen injection strategies discussed above mostly aimed at generating a relatively well mixed charge. To allow a larger degree of fuel-air mixture stratification, close-coupled injection and

ignition strategies were proposed [76], namely the plume-head and plume-tail ignition. Both strategies utilize a late SOI—the plume-head ignition is triggered soon after the SOI, whereas the plume-tail ignition strategy triggers ignition of the jet just after the end of injection. The exact SOI timing and injection duration can be varied depending on engine requirement but the common SOI timings are after 50° and 20° CA BTDC for high and low load, respectively [76]. The results highlight the importance of ignition location within the jet. In a 1.05 L single-cylinder engine with CI combustion chamber geometry [76,77], at low load and 200 bar injection pressure, the plume-head ignition was reported to achieve the highest ITE of ∼38% and lowest NO$_x$ emissions below 500 ppm. The NO$_x$ emissions for plume-tail ignition at the same load can exceed 1000 ppm. In contrast, at high load, NO$_x$ emission levels can be less than 500 ppm for both ignition methods decrease with retarded injection timing and higher EGR. Nevertheless, the plume-tail ignition shows considerable advantages with respect to ITE at high load—at optimized injection and ignition timing, the plume-tail ignition can reach 48% ITE compared to that of 37% reported for the plume-head ignition. The governing mechanisms behind these combustion strategies were studied by Roy et al. [78,79] in a 0.31 L single-cylinder optical engine using 50 bar hydrogen injection pressure. It was found that the plume-head ignition has considerably lower peak cylinder pressure and its peak rate of heat release is approximately 60% lower than that of plume-tail ignition, indicating a diffusive combustion. Furthermore, the coefficient of variation of IMEP was found to be 24%, compared to 7% for plume-tail ignition, implying an unstable engine operation for the plume-head ignition strategy. Though not fully understood, local equivalence ratio measurements using spark-induced breakdown spectroscopy show that the mean local ϕ for plume-head ignition is relatively low, thus explaining the unstable combustion.

Overall, the literature suggested that the ideal in-cylinder fuel distribution before SI consists of a sufficiently fuel-rich region near the spark plug to ensure reliable and fast flame initialization but a fuel-lean mixture close to the wall to minimize wall heat losses [80]. The fuel and air mixing process of high pressure jets is understood to a certain extent, from a number of studies using flow visualization and simulation works [30,34,36,37]. In essence, the fuel concentration and flow field were visualized under non-reactive conditions in a motored engine by planar laser-induced fluorescence and particle image velocimetry measurement, respectively. When a hydrogen jet was injected towards the engine side wall with injection timing between 137–120.5° CA BTDC, it was observed to produce a wall-jet vortex after wall impingement. The jet was then redirected rapidly and slowed down by the air entrainment, followed by an upward push by the engine piston. It was also observed that a more stratified mixture can be formed with less tumble flow within the chamber. It is noted that injection angle, injection timing, injector nozzle number and piston geometry, etc, also have a significant impact on the final mixture formation.

Although the hydrogen DI SI engine concept mitigates several issues of the PFI configuration, the efficiency is still inferior to contemporary diesel CI engines. This can partially be attributed to the limitation of knocking and pre-ignition, which limit the compression ratio applicable for this combustion mode. Also, the combustion phasing might be sub-optimal since the number of combustion kernels in this combustion mode is usually limited by a single spark plug in the engine, leading to a slower early stage combustion. Therefore, the hydrogen jets from a multi-nozzle injector cannot be ignited simultaneously, limiting the combustion speed. A potential approach to mitigate this issue is seen in the concept of dual-fuel H2DDI, utilizing flame-kernels from pilot fuel auto-ignition to ignite the hydrogen jets.

6. Dual-Fuel High Pressure Direct Injection Compression-Ignition Engine

As discussed earlier, achieving hydrogen auto-ignition without any ignition assistance, such as the HCCI mode or diesel-like diffusion combustion, is challenging due to the high auto-ignition temperature of hydrogen. To circumvent this limitation, a small amount of diesel pilot fuel is injected into the combustion chamber as an ignition source for the high pressure gas jet. Although a similar injection strategy was proposed back in the 1980s [81], most of the studies used CNG as the primary

fuel. Dual-fuel compression ignition with the DI of hydrogen has not been demonstrated to date. These studies typically inject a small amount of pilot diesel fuel prior to gas DI, in order to create a high temperature environment to assist the gaseous fuel ignition to achieve CI engine diffusion-like combustion. This novel combustion mode for hydrogen ICE can alleviate charge knocking and allows the engine to operate at a higher compression ratio to improve thermal efficiency up to levels that are comparable to contemporary CI engines. Since CNG has a comparable auto-ignition temperature to hydrogen, reviewing the results of CNG dual-fuel DI research can provide useful insights into the underlying mechanisms of this combustion mode, including the understanding of the gas jet interaction with the pilot diesel fuel. The effect of different operating parameters, for instance injection timing, injection pressure, interactions between the two fuels and ambient conditions will be discussed. The implications for changing the fuel from CNG to hydrogen are summarized later in this section. Dual-fuel DI engines are usually realized by employing an integrated concentric injector providing separate flow paths to independently admit both gas and diesel fuels from the same injector unit. Two separate injectors for the two fuels can also be used. As an alternative, earlier studies [82,83] investigated the possibility of external mixing of CNG and diesel before injection. These studies showed that mixing of CNG into diesel fuel lengthens the ignition delay, leading to an excessive pressure rise rate, especially at low load. Therefore, this approach did not attract attention in later studies and will not be discussed in depth.

In dual-fuel DI combustion mode, the nozzle and injector orientation was shown to play an essential role in improving the combustion process since it defines the interaction between the pilot fuel and gas jets. Figures 3 and 4 show the schematic of the axial cross section and top view of the dual-fuel DI jet orientation with a concentric injector, respectively [81]. The injection vertical angle is defined as the angle between the jet axis and the cylinder head in the axial cross-sectional plane, while the interlace angle is defined as the angle between the gas and diesel jet axis of a concentric injector on the top plane. It should be noted that the interlace angle is diverging from the concentric injector in Figure 4, however, depending on the injector configuration, it can be arranged as parallel or converging.
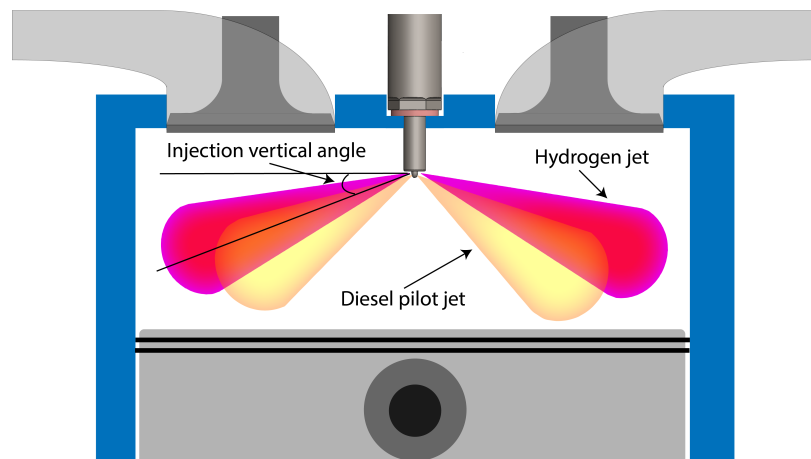

Figure 3. Schematic of the dual-fuel DI concentric injector jet configuration on the axial cross-sectional plane. The injection angle is defined as the angle between the jet axis and the horizontal axis in this plane. Reproduced from Trusca [81].
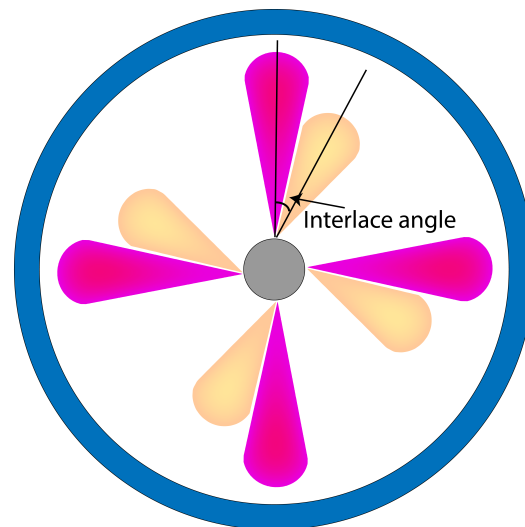
Figure 4. Schematic of the dual-fuel DI concentric injector jet configuration on the top-plane. The interlace angle is defined as the angle between the two jets' axes on this plane. Reproduced from Trusca [81].

Early investigations by Miyake et al. [83] in 1983 demonstrated a higher BTE of CNG-diesel dual-fuel DI engine than the contemporary diesel engines at the time. A modified large bore (420 mm) four-stroke single-cylinder diesel engine with two separate injectors was used. Diesel pilot jets were injected from the periphery of the cylinder in a radial direction and the gas injector was mounted in the center, perpendicular to the cylinder head. Using an injection pressure of CNG at 250 bar, only 5% of diesel fuel in the total energy input was required to achieve 85% and 100% of the engine full load.

Later studies demonstrated the significant influence of injection timing of diesel and gas jets on engine performance in the dual-fuel DI mode. Trusca [81] performed engine testing using a modified 1.2 L single-cylinder diesel engine, operated at 1200 rpm at low and medium loads, using an integrated concentric dual-fuel injector. Gas jet injection began just before the end of pilot diesel injection, which accounted for 5% of the total energy share. The relative SOI, defined as the delay between the start of diesel and gas injections, was approximately 10° CA. It was found that an early pilot diesel injection at $\sim$25° CA BTDC can achieve the highest peak cylinder pressure, across various injection pressures and loads studied. Delayed injection resulted in a reduced peak cylinder pressure. This was attributed to a delayed pilot-fuel ignition, which leads to a later combustion phasing of the gaseous fuel. Nevertheless, the later combustion phasing may be compensated by a decrease in other engine losses, as engine efficiency was found to be insensitive to SOI timing for most cases at the same injection pressure and engine load [81]. A more recent optical investigation using schlieren imaging by Dai [84] in a constant-volume chamber under non-reactive conditions used two parallel injectors (Figure 5) to investigate the importance of relative SOI between the jets. Findings suggested that the gas jet should not be injected too early before the auto-ignition of diesel, as it was observed to rapidly mix with the diesel jet, which may lengthen diesel ignition delay due to the entrainment of colder gaseous fuel instead of hot oxidizer required for ignition. On the other hand, late gas injection may result in misfire of the gas jet, because the hot diesel combustion products of typically short pilot injections rapidly lean out and cool. This was later confirmed by Ishibashi and Tsuru [85] under reactive conditions using an optically-accessible rapid compression and expansion machine (RCEM) at 300 rpm to observe the interaction of diesel and gas jets from single-hole injectors with a converging arrangement. The effect of injection timing was demonstrated by altering the diesel injection timing at a fixed gas injection timing (i.e., 4°, 2°, 0° CA relative SOI with pilot diesel being injected first). An improved performance was observed at the medium temporal separation of injections (i.e., 2° CA relative SOI) of both fuels, with slightly reduced unburned hydrocarbon and NO_x emissions. When both fuels were injected simultaneously, both fuel jets merged and the diesel fuel rapidly mixed with the gaseous fuel before

ignition occurred. This increased the ignition delay and induced a high peak heat release rate due to the large mass of accumulated combustible charge formed by the time of ignition.
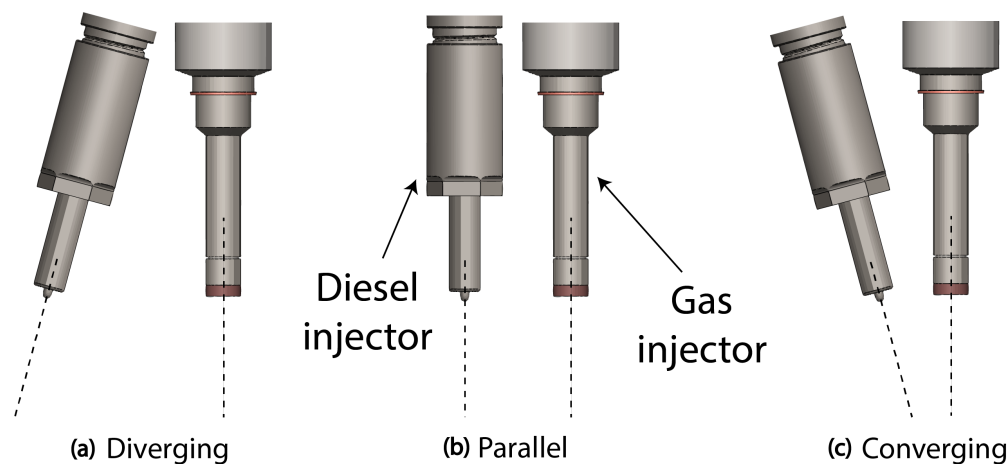

Figure 5. Two co-axial injector Dual-fuel DI configurations, with (**a**) diverging, (**b**) parallel and (**c**) converging nozzle orientation. The figure is not drawn to scale.

Douville [86] performed testing using the same engine and injector setup as Trusca [81] and investigated the effect of CNG injection pressure on engine efficiency and emissions. The injection pressure of CNG was varied from 100 to 140 bar. Over this range, the results at low and medium loads indicated only minor effect of injection pressure on thermal efficiency, similar to conventional diesel operation. Nevertheless, higher engine loads could be reached at higher injection pressures. On the other hand, an increase of NO_x emissions was detected with increasing gas injection pressure for all tested loads. This conclusion was confirmed in later studies for a larger range of injection pressure by Trusca [81] and McTaggart-Cowan et al. [87]. However, these studies reported faster combustion leading to a moderate enhancement of engine efficiency with an increasing injection pressure from 130 to 170 bar and from 280 to 400 bar, respectively. This is inconsistent with the results by Douville [86]. Nevertheless, no further increase in efficiency was observed at injection pressure exceeding 480 bar. At this optimized condition, a BMEP of 22.5 bar and BTE exceeding 40% were reached [87]. While these studies provide a good starting point for parametric analysis, the understanding of the influence of injection pressure on combustion and efficiency is limited and more work with optical diagnostics is needed for further understanding. The study by Dai [84] showed that both injection and ambient pressure affect gas jet penetration similarly to diesel jet. The penetration increases with higher injection pressure but decreases with higher ambient pressure.

The interaction between the pilot fuel and gas jet was studied optically under room conditions employing schlieren imaging by White [88]. A range of jet alignments was investigated as demonstrated in Figure 5 (i.e., diverging, parallel as well as converging). As expected, a converging configuration promotes interaction between the diesel and gas jets. However, in a converging arrangement with large angle between the jets, the gas jet was observed to pass through the diesel liquid jet and the development of a conical gas jet was not affected by the interaction with diesel jet. Under an assumption that a maximized overlapping of diesel and gas jets after the auto-ignition of diesel fuel will yield the best performance, a converging injector configuration with small angle (a few degrees) was recommended [88]. The effect of the dual-fuel jet interaction under engine-relevant reactive conditions was studied by Fink et al. [89,90] in a RCEM. Different injector orientations were used to change the degree of jet interaction—the gas injection angle was changed by rotating the injector while the diesel jet was fixed. The results confirmed non-reactive predictions that ignition is improved when the two jets overlap, especially at low ambient temperature. The combustion was found to be unstable when parallel jet arrangement was used. Although a large extent of gas jet overlapping with the pilot diesel lowers diesel combustion intensity, the ignition of the gas jet

occurs earlier. The interlace angle, as shown in Figure 4, is another degree of freedom in dual-fuel DI configuration to induce various level of interactions between the diesel and gas jets but it is more relevant for concentric injectors. Similar to the injector vertical configuration, a previous simulation study [91] showed that when the interlace angle is reduced from 30° to 15°, the two jets have a larger overlapping area, leading to an increased combustion rate with a trade-off of NO_x emissions.

Fink et al. [90] investigated the effects of ambient pressure and temperature on dual-fuel combustion using shadowgraphy and OH-chemiluminescence in a RCEM. It was found that the ignition of gas jet becomes possible at a wider range of injector orientations and relative SOIs with an increasing ambient pressure and temperature (i.e., from 780 to 920 K). At a fixed slightly diverging injection configuration and a negative relative SOI (i.e., gas jet is being injected first), the ignition delays relative to their SOIs decrease for both jets with an increase in ambient temperature. However, the temporal difference between the diesel fuel auto-ignition and ignition of the gas jet increases. This was attributed to an earlier ignition of diesel fuel, which therefore occurrs closer to the injector orifice—at a larger distance from the gas jet. It should be noted that this observation may only be applicable to a specific injector configuration. The study also observed that heat release rates between different ambient temperatures show a similar profile at the same level of premixing but the peak heat release rate increased with higher ambient temperature.

Despite the wealth of studies, the interplay between injector configuration, ambient conditions, combustion premixing and heat release rate is not completely understood. Therefore, additional dedicated studies under a wider range of conditions and configurations both in engines and optically-accessible test rigs are needed. It should be noted all of the above studies used CNG as the gaseous fuel—the potential of dual-fuel DI combustion mode with hydrogen remains largely unexplored (i.e., H2DDI). However, the above studies demonstrated the potential to reduce the use of diesel significantly compared to diesel-ignited hydrogen PFI, where pre-ignition and knocking limit hydrogen to 6–25% of total energy share at high load as discussed above. One of the obvious advantages to use hydrogen over CNG is that carbon-based emissions will be reduced significantly. Although pilot fuel potentially forms soot, the close-coupled high velocity hydrogen jet could enhance mixing within the chamber, which can subsequently lead to enhanced soot oxidation and suppress soot formation processes, similar to diesel post-injection strategy [92,93]. The larger speed of sound and higher calorific value of hydrogen largely compensate for an order of magnitude lower density relative to CNG, therefore, requiring only $\sim$20% longer injection duration at 249 bar injection pressure ratio and 353 K fuel temperature [94]. This is because the rate of fuel energy input is dependent on the fuel's energy content and injection mass flow rate, as will be discussed in the next section. A few studies [81,95] have investigated the effect of hydrogen-CNG blend in dual-fuel DI combustion using heavy-duty engines and integrated dual-fuel injectors. Gas injection duration was adjusted to achieve the same engine load as when operating on neat CNG. The results show good agreements that carbon-based emissions, for instance unburned hydrocarbon, CO and CO_2, decrease with a higher hydrogen share but with a trade-off of increasing NO_x emissions. At low load, a higher peak heat release rate was observed when a hydrogen-CNG blend was used, with the opposite trend at high load. This is because the combustion rate is limited by chemical reaction at low load and the addition of hydrogen can provide reactive species (e.g., H and OH) in the reaction zone to widen the mixture's flammability range, leading to enhanced combustion rate [95]. However, the early stage combustion process is limited by the availability of fuel at high load, due to the lower density of hydrogen. Gas ignition delay decreases with high hydrogen share for all loads, indicating an improvement on fuel ignitability. Furthermore, combustion stability can be significantly improved at low load with increasing hydrogen addition, attributable to a more complete consumption of fuel.

The hydrogen dual-fuel H2DDI combustion concept shows the potential to facilitate a broad market penetration of hydrogen fueled ICE in different applications. However, the underlying processes and implications for the engine performance are not well understood, therefore, additional research is required to facilitate its mass adoption. Among others, the ARENA in Australia along with

a number of academic and industry partners are leading several projects to investigate the potential of dual-fuel H2DDI mode [96]. Studies in engine testing, optical diagnostics and numerical simulation will be produced in the next few years, to advance the understanding of the governing mechanisms and to optimize engine performance of this engine mode.

7. Non-Premixed Hydrogen Diffusion Combustion

An important intermediate step towards optimized hydrogen DI ICE performance and emissions is to understand the characteristics of hydrogen jets under non-reactive and reactive conditions. Fundamental studies of hydrogen jet combustion are limited; nevertheless, studies in constant-volume combustion chamber with only auto-ignition have identified some of the hydrogen jet features. Naber and Siebers [97] reported that injection pressure and nozzle size have a negligible effect on ignition delay, as it is more sensitive to ambient conditions. A decrease of ignition delay from ∼5–0.2 ms was reported, with an increasing ambient temperature from 970 to 1200 K at a fixed initial fuel temperature, ambient density and O_2 concentration of 450 K, 20.5 kg/m^3 and 21 vol%, respectively. However, the study from Tsujimura et al. [98] found a decrease of ignition delay from 2 to 0.5 ms, when increasing the nozzle diameter from 0.3 to 1 mm, at 1000 K ambient temperature. They attributed this finding to the quantity of mixture and the turbulence length-scale generated during injection. However, in the absence of high-fidelity optical diagnostics and simulations results, the underlying mechanisms behind these findings are not well understood. Also, no literature information on the flame structure of a combusting hydrogen jet and its interaction with pilot-fuel jet under engine relevant conditions is available up to date. Future work with advanced optical diagnostic techniques measuring the fuel distribution, turbulence conditions and reactive species evolution would certainly provide useful insights into reactive hydrogen jet development.

Gas Jet Model

Since hydrogen jet combustion in non-premixed diffusion combustion mode relies significantly on high pressure jet characteristics, the characteristics of the gas jet need to be understood. The jet features are equally important, if hydrogen is burned in partially premixed combustion mode, as the hydrogen jet features affect fuel and air mixing as well as fuel stratification. Figure 6 shows a widely accepted turbulent transient gaseous jet model, known as the vortex ball model, proposed by Turner in 1962 [99,100]. If a round nozzle is used, the gaseous jet in an unconfined environment is assumed to have a conical shape with axisymmetric head vortex and some minor irregularities. Most of the air entrainment is expected to occur in the steady-state region, with Gaussian velocity profiles in the fully developed region upstream of the head vortex [100]. The jet penetration, defined as the axial distance between the jet tip and injector nozzle, alongside with the jet cone angle, were shown to have a strong influence on ambient air entrainment.
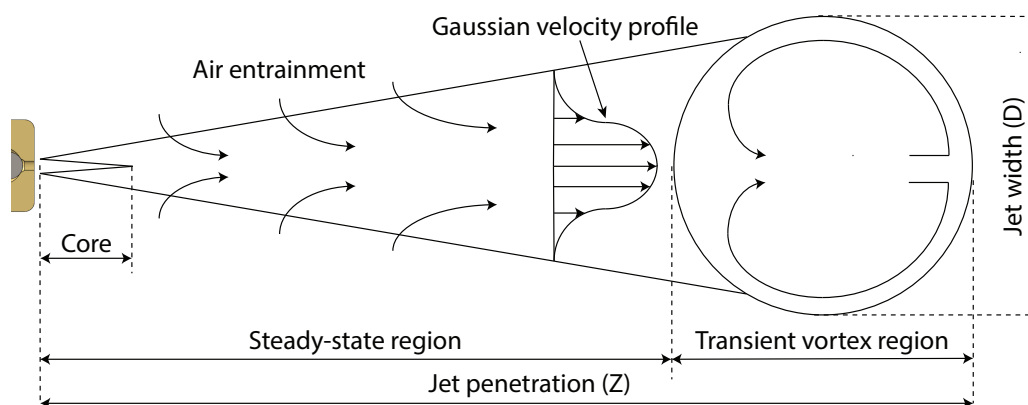

Figure 6. The vortex ball model of turbulent transient gaseous jet. Reproduced from Ouellette [100].

As discussed earlier, increasing the injection pressure increases fuel density in reservoir and fuel mass flow rate during the injection, which implies that HPDI of hydrogen has potential to achieve a high engine load. Usually, hydrogen in the jet can be described as an ideal gas and the flow is considered as an isentropic process, indicating no heat transfer and frictionless system [98]. The flow pattern in the core region depends on the pressure ratio across the nozzle—the jet can be considered as underexpanded when sonic condition is reached and flow is choked at nozzle exit. Literature distinguishes the moderately underexpanded and highly underexpanded jets, which occurs when the pressure ratio between the reservoir and ambient exceeds 2 and 3.85, respectively [101]. For a moderately underexpanded jet, a shock normal to the flow direction is formed with repeated diamond-shaped oblique shocks established in the core region [101]. On the other hand, for a highly underexpanded jet, the hydrogen gas will rapidly accelerate upon leaving the nozzle. The large difference in gas pressure after exiting the nozzle results in the formation of expansion waves in a process described by the Prandtl-Meyer expansion fan [102]. These waves grow until the boundary is generated to resist the jet expansion and to reflect the expansion waves as compression shock waves. A barrel-shaped shock with a Mach disc is formed downstream the injector nozzle due to the coalescence of compression shock waves, as shown in Figure 7 [100]. The diameter and distance of the Mach disc from the nozzle exit increase with the pressure ratio across the nozzle as well as nozzle diameter [98]. It is noted that the highly supersonic flow and shock boundary prevent any gas exchange within the barrel-shaped shock [102]. Therefore, the formation of a barrel shock can considerably affect the overall fuel and air mixing.
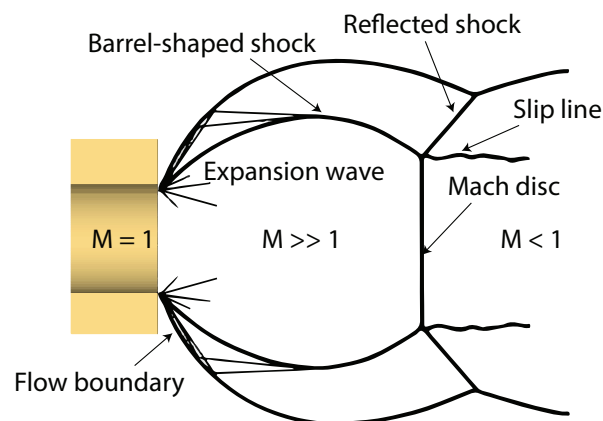

Figure 7. Schematic diagram of the highly underexpanded gaseous jet, with shock formation downstream of the injector nozzle. Reproduced from Ouellette [100].

However, the influence of combustion on the gas jet model under reactive engine conditions still has to be explored. It is also noted that in realistic applications, the hydrogen jet will inevitably interact with the engine chamber wall. Therefore, flame-wall interaction effect also needs to be considered, constituting a more complex scenario than free jet. Literature investigating hydrogen jet interaction with walls is scarce. Examples from liquid fuel jet research include optical investigations studying jet impingement on different wall geometries at a defined distance from the nozzle, for instance a plane flat wall or a confined wall [103,104].

8. Fuel System for High Pressure Hydrogen Injection

One of the major obstacles in commercializing hydrogen DI or dual-fuel DI engine is the lack of commercially available hydrogen injection hardware. An integrated two-fuel HPDI injector is marketed by the Westport Innovation Inc. This injector was used to inject CNG in the studies by Douville [86] and Trusca [81], and so forth. Despite this injector was mainly developed for CNG, a few studies [81,95] successfully used the injector for a hydrogen-CNG blend. This injector consists of two concentric spring-loaded needles, which allows a separate control of the gas and liquid fuel

injections. The internal structure and more information about this injector can be found in the study by Trusca [81]. The Westport HPDI technology advanced to a tank-to-tip system, known as HPDI 2.0 and it is utilized commercially for heavy-duty truck applications in the US, Europe and Australia [87,105]. The injection pressure limit of the HPDI 2.0 system is around 600 bar for both diesel and CNG. Previous studies [89,90] employed a prototype injector by L'Orange from Germany to inject CNG at high pressure of up to 330 bar. However, no information about the applicability of this prototype for hydrogen injection is available. Furthermore, in an engine application, such injector will have to be combined with a second injector to deliver pilot diesel fuel.

The challenges of developing a hydrogen injector was documented in a publication by Welch et al. [94]. One of the main challenges is the low lubricity and viscosity of hydrogen. The low lubricity leads to increased friction wear. The low viscosity leads to reduced internal damping resistance of moving components, resulting in a stronger impact when moving parts reach their final positions, especially when the needle impacts the seat during the injector closing. This may also lead to resonant effects, part disassembly, material failures, wear and possible needle bouncing. An application of dry lubricants or low friction coating on surfaces could be used to alleviate this issue. Additionally, due to the high diffusivity of hydrogen, it can permeate through various materials. As a consequence, the epoxy material used in piezoelectric actuator can be delaminated, when the pressure is relieved, leading to an internal short circuit. Hydrogen is also known to cause embrittlement of common engineering steels, which reduces the injector durability [106].

Various prototype injectors for gas only hydrogen HPDI are documented in the literature. For example, Westport and its partners reported two generations of development of hydrogen only HPDI injector by modifying the design of CNG DI injectors. The first generation used solenoid actuation, which was upgraded to piezo-actuation in the second generation. The performance of these injectors was extensively tested by the Argonne National Laboratory [30–39]. Concurrently, the Japanese National Traffic Safety & Environment Laboratory (NTSEL) program developed an electrohydraulic-actuated injector to achieve hydrogen only HPDI and applied it in a number of studies within the program [72,74,75]. The schematic and operation principles of these injectors can be found in previous studies [80,94,107]. A brief summary of their characteristics is given below.

1. Electrohydraulic-actuated (NTSEL): This type of injector requires high-pressure hydraulic fluid (usually diesel fuel) for actuation. The injection pressure is limited to 200 bar. During the injection actuation, the electronically-triggered solenoid acts on the pilot-needle to relieve diesel pressure at the upper part of the injector, reducing hydraulic force that pushes the needle into its seat. Therefore, the high pressure hydrogen can lift the needle and the injection begins. In this design, the diesel pressure needs to be high enough to ensure needle sealing in closed position. It also provides lubrication to some of the injector moving parts. However, the long opening transient duration due to the inertia of hydraulic actuation system might be undesirable in some applications.

2. Solenoid-driven (Westport): The first generation Westport hydrogen DI technology is entirely driven by a solenoid. The direct solenoid actuation imposes an injection pressure limit, which is the lowest among the listed injectors at 150 bar. In addition, a serious durability issue was reported and attributed to the lack of needle motion control required to minimize the needle impact into the seat. Hoerbiger Valve TEC GmbH has also developed a similar solenoid-driven hydrogen DI injector but with a maximum injection pressure of 100 bar [72].

3. Piezo-driven (Westport): This second generation injector with maximum injection pressure of 250 bar is directly driven by a piezoelectric crystal, using analog voltage to proportionally control the needle displacement, enabling a very fast response time. It has a short opening transient duration of 0.5 ms, similar to their solenoid-driven design but only with 35% of that of the NTSEL's injector. Additionally, the injector lifetime is improved by the flexible control of the needle velocity, which can be decelerated at closing to reduce impact. Multiple injections can also be performed.

Many of the commercial injectors for gasoline direct injection (GDI) engines feature directly actuated needle and can therefore be operated with gaseous fuels. The durability due to the poor lubricity of gaseous fuels is the main concern; nevertheless, several researchers have successfully utilized GDI injectors for hydrogen DI injection, with no significant gas leakage reported [43,78,79,102]. Although most of these studies tested the injection pressure of hydrogen only up to 100 bar, the commercialization of higher GDI injection pressure injectors might raise possibilities to utilize a higher gas injection pressure. Due to the durability concerns, such modifications are only applicable for research purposes, where the injector does not need to be operated continuously for a long period of time. For fundamental jet research purposes, a typical multi-hole GDI injector can be modified to a single nozzle configuration to avoid complexities that can arise from jet-jet interaction. Figure 8 shows the author's design of a single-nozzle GDI injector modification, similar to those in References [102,108,109]. A part of the original injector tip is removed and a customized cap with single nozzle is threaded onto the injector shaft, with an o-ring to prevent hydrogen leakage. This approach is relatively cost effective and the nozzle geometry can be simply modified for different test requirement, even multiple nozzles can be featured. Material suitability suggests the use of Viton elastomer since hydrogen induces swelling in lower-grade rubber components [106]. Great care needs to be taken at the needle seat, as needle valve sealing is determined by surface finish—precision of less than 1 micron is recommended [107]. The clearance around the needle should be large enough to ensure sufficient flow rate and the nozzle inner wall should have a smooth surface finish to minimize flow disturbance. A spherical contact between the needle and inner cap surface might improve sealing integrity and prolong the injector lifetime. The cap should be made of softer materials (e.g., brass) than the needle, since the material can deform when in contact with the needle due to its ductility to ensure a mating face for sealing purposes [102]. Nevertheless, soft material will raise durability issues—Rogers [102] reported a lifetime of only several thousand cycles for the customized cap before the sealing surface starts rolling over and alters the nozzle flow behavior.
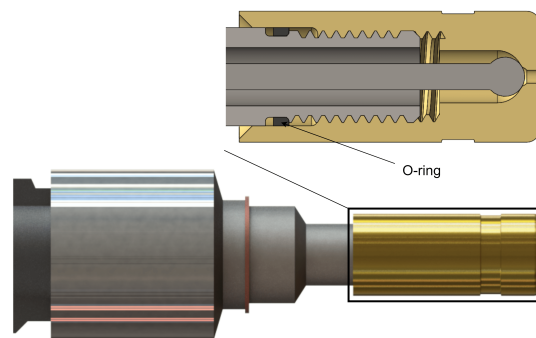

Figure 8. GDI injector modification design with a brass coaxial single-nozzle cap and its detailed section view.

8.1. Injector Design Considerations

The fuel injector design plays an important role in engine performance and has to be carefully considered. The injector characteristics, such as maximum injection pressure and nozzle size, directly affect the fuel injection rate and mixing and also govern the fuel injection quantity. Consequently, the injector configuration influences the heat loss through flame-wall interaction, and so forth.

8.1.1. Injection Rate

Under choked flow conditions, the maximum flow velocity and thus the maximum mass flow rate ($\dot{m}_{\max}$) across the nozzle are limited by the speed of sound. By assuming that the enthalpy is only temperature dependent and incorporating the compressible flow theory under choked condition, the maximum mass flow rate can be approximated using Equations (1)–(3), with the subscripts o and superscript $*$ representing the infinite reservoir and speed of sound condition, respectively [98].

These equations should be applicable for different nozzle geometries, using the nozzle area at sonic condition. The validity of these equations for high pressure hydrogen injection was tested by measuring the mass flow using a straight single-nozzle electrohydraulic-actuated injector by Tsujimura et al. [98]. A range of pressure ratios and nozzle diameters was tested and the agreement between the measured and calculated average mass flow rates was better than 90% in most cases. The agreement becomes worse, if the injection duration is shorter than 5 ms, attributed to the needle opening transient.

$$\dot{m}_{\max} = \rho^* u^* A^* \tag{1}$$

$$= \left[\rho_o \cdot \left(\frac{2}{\kappa + 1} \right)^{1/(\kappa-1)} \right] \left[\sqrt{\frac{2\kappa}{\kappa + 1} \frac{P_o}{\rho_o}} \right] A^* \tag{2}$$

$$= P_o A^* \sqrt{\frac{\kappa}{R_o T_o}} \cdot \left(\frac{2}{\kappa + 1} \right)^{(\kappa+1)/2(\kappa-1)} \tag{3}$$

where A = area

P = pressure

ρ = density

u = velocity

T = temperature

R = specific gas constant (i.e., universal gas constant/molar mass)

κ = specific heat ratio

Equation (3) was used to calculate the sensitivity of maximum injection rate to nozzle diameter and injection pressure (Figure 9a) and to estimate the theoretical minimum injection duration for engine operation (Figure 9b), assuming a single-hole injector. The fuel temperature was fixed at 298 K and a minimum injection pressure of 150 bar was postulated to ensure that a critical pressure ratio condition of 2 is reached for choked flow and underexpanded jet, assuming a back pressure representative of conditions around the top dead center in CI engines. The injection duration was derived from the nozzle mass flow using an injection quantity of ~7 mg of hydrogen per injection, assuming the load and efficiency from a previous hydrogen DI SI study [73] in a 2.2 L four-cylinder engine (i.e., IMEP of 6 bar and ITE of ~45% at 2000 rpm). The injection rate of hydrogen jet, as shown in Figure 9a, increases proportionally to injection pressure and with the square of nozzle diameter. The indicative minimum injection duration, as shown in Figure 9b, therefore decreases inversely proportional to higher injection pressure and quadratically with larger nozzle diameter. Despite the low density of hydrogen, with a nozzle diameter of 1 mm, the theoretical minimum injection duration as short as 5° CA can be achieved at injection pressure of 350 bar. At moderate injection pressure of 200 bar, the flow rate is sufficient to deliver the fuel mass within 10° CA. However, it should be noted that the calculation is just a theoretical indication using the maximum flow rate and the actual injection duration is expected to be longer due to the injector opening and closing transient [98]. Apart from delivering the required fuel quantity for a certain load, nozzle size and arrangement as well as the injection pressure need to be optimized for the engine geometry in order to achieve the best performance.
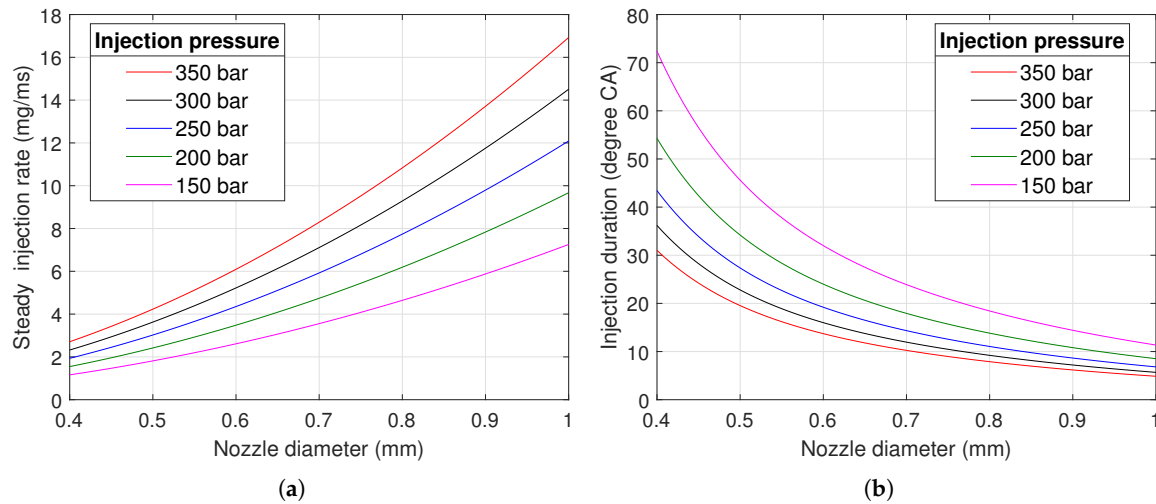
Figure 9. Theoretical (**a**) maximum steady injection rate and (**b**) minimum injection duration required for injecting 7 mg hydrogen at 2000 rpm at different injection pressures and nozzle diameters.

8.1.2. Axial Jet Penetration

Hill and Ouellette [110] developed a widely used jet tip penetration (Z_t) prediction model for a gaseous jet as a function of time assuming the conservation of momentum. The validity of this model has been demonstrated for highly underexpanded jets with pressure ratio of up to 70, unaffected by the barrel-shaped shock. This model, described by Equations (4) and (5) [110,111], assumes a constant momentum discharge rate and density during the injection, as well as self-similar jet velocity and mixing distribution. Since the underexpanded jet flow is choked, the nozzle exit velocity (subscript *e*) is assumed to be the sonic speed [112]. The subscript *a* represents the ambient condition and Γ is a constant dependent on jet cone angle, as shown in Equation (6) [110]. The sensitivity of Γ to jet cone angle is small. A 50% increase of *s* from 0.2 to 0.3 only decreases Γ from 3.04 to 2.89 (i.e., 5% decrease). Hill and Ouellette [110], therefore, proposed that a universal estimation of 3 for Γ can be used. A study [102] in a constant-volume chamber has also shown a small sensitivity of fully developed underexpanded jet spread angles to ambient conditions. Regardless of the fuel type and pressure ratios from 3 to 12, the jet spreading angles remained similar in the range of 22°–28°.

$$Z_t = \Gamma \left(d_e \times u_e\right)^{1/2} \times \left(\frac{\pi}{4} \frac{P_o}{P_a} \frac{R_a}{R_o} \frac{T_a}{T_o} \left(\frac{2}{\kappa_o+1}\right)^{\frac{1}{\kappa_o-1}}\right)^{1/4} t^{1/2} \tag{4}$$

$$= \Gamma \left(d_e\right)^{1/2} \times \left(\frac{\kappa_o \pi}{4} \frac{P_o}{P_a} R_a T_a \left(\frac{2}{\kappa_o+1}\right)^{\frac{\kappa_o}{\kappa_o-1}}\right)^{1/4} t^{1/2} \tag{5}$$

$$\Gamma^4 + \frac{1.92(1-s)^2}{\sqrt{\pi}(2-s)s^3}\Gamma^2 - \frac{24}{\pi(2-s)s^3} = 0 \tag{6}$$

where t = time after SOI

d = diameter

s = ratio of jet width to jet penetration distance (D_t/Z_t)

In reality, the effective pressure (P_{eff}) at the nozzle exit is less than the fuel supply reservoir pressure due to the high compressibility of gas flow [113], which is not considered in Equation (4). An estimation of the effective pressure depending on the reservoir pressure, ambient pressure and other gas properties was developed by Hajialimohammadi et al. [111] based on the shock tube diaphragm

rupture process as described by Equation (7). The effective pressure ratio to the ambient pressure (P_{eff}/P_a) in Equation (7) can be approximated using the Newton-Raphson method. This effective pressure can then be substituted to Equation (4) to predict jet tip penetration accounting for the pressure loss at nozzle exit, as shown in Equation (8). Therefore, the jet penetration mainly changes with the injection pressure and nozzle exit diameter at an unchanged operating condition and depends on the gas properties. Table 2 shows a comparison of the effective pressure ratio for hydrogen, helium, methane and nitrogen, using a range of reservoir/ambient pressure ratios. A typical CI engine ambient condition around top dead center was assumed, with ambient density, pressure and temperature at 20.8 kg/m^3, 60 bar and 1000 K, respectively [104]. The reservoir temperature was set at 298 K. It is noted that the effective pressure still increases with the reservoir pressure but at a lower rate and methane has a higher pressure loss than hydrogen at the same condition. Also, the effective pressure ratio decreases with both increasing gas's molar mass and specific heat ratio, as seen from the comparison of different gases in Table 2.

$$1 + \left(\frac{u_o^*}{u_a^*}\right)\left(\frac{\kappa_a - 1}{\kappa_o - 1}\right) - \left[\left(\frac{u_o^*}{u_a^*}\right)\left(\frac{\kappa_a - 1}{\kappa_o - 1}\right)\right]\left(\frac{P_a}{P_o}\right)^{\frac{\kappa_o - 1}{2\kappa_o}}\left(\frac{P_{eff}}{P_a}\right)^{\frac{\kappa_o - 1}{2\kappa_o}} - \left(\frac{P_{eff}}{P_a}\right)^{\frac{\kappa_a - 1}{2\kappa_a}} = 0 \qquad (7)$$

$$Z_t = \Gamma\left(d_e\right)^{1/2} \times \left(\frac{\kappa_o \pi}{4}\frac{P_{eff}}{P_a}R_a T_a \left(\frac{2}{\kappa_o + 1}\right)^{\frac{\kappa_o}{\kappa_o - 1}}\right)^{1/4} t^{1/2} \qquad (8)$$

Table 2. Calculated effective pressure ratio for different reservoir pressure ratios for hydrogen, helium, nitrogen and methane.

Reservoir Pressure Ratio (P_o/P_a)	Effective Pressure Ratio (P_{eff}/P_a)			
	Hydrogen	**Helium**	**Methane**	**Nitrogen**
2	1.58	1.46	1.34	1.27
4	2.46	2.09	1.77	1.59
6	3.17	2.55	2.07	1.80

Accounting for the difference in effective pressure ratio, Table 2 suggests a faster penetration of hydrogen jet relative to nitrogen or methane. This is demonstrated in Figure 10, which compares the theoretical jet penetration of hydrogen to methane as conventional gaseous fuel in HPDI applications. Two comparisons are demonstrated—Figure 10a shows the jet penetration for a variation of injection pressures at a fixed nozzle diameter of 1 mm. Ambient condition was assumed the same as that in Table 2. A comparison with increased hydrogen injection pressure to match the energy flow of methane jet is presented as well. Figure 10b compares the jet penetration for a variation of nozzle diameters at a fixed injection pressure of 150 bar. Similarly, a comparison with increased hydrogen jet orifice diameter to match that of the methane jet's energy flow rate is presented. It is noted that hydrogen with 158 bar and 369 bar injection pressure provide the same theoretical energy flow rate as methane at 150 bar and 350 bar, respectively; nozzle diameters of hydrogen injection need to be increased to 1.03 mm and 1.54 mm for the same theoretical energy flow rate as methane injection with 1 mm and 1.5 mm nozzle diameters, respectively. Equation (8) and Figure 10 show a higher sensitivity of jet penetration to nozzle diameter than to injection pressure, as confirmed by schlieren imaging experiments [98]. In addition, hydrogen jet indeed penetrates faster than methane under the same conditions, which is mainly attributed to a difference in effective pressure ratio, as shown in Table 2. Therefore, the injection pressure of methane jet has to be nearly doubled to provide the same penetration as hydrogen jet. Previous experiments by Rogers [102] and large eddy simulation by Hamzehloo and Aleiferis [114] have validated the faster jet tip penetration of hydrogen than methane at the same pressure ratio. This needs to be considered when transferring current knowledge from CNG dual-fuel DI combustion

to hydrogen. However, hydrogen combustion under engine conditions may affect the jet penetration behaviour, which needs to be further verified.
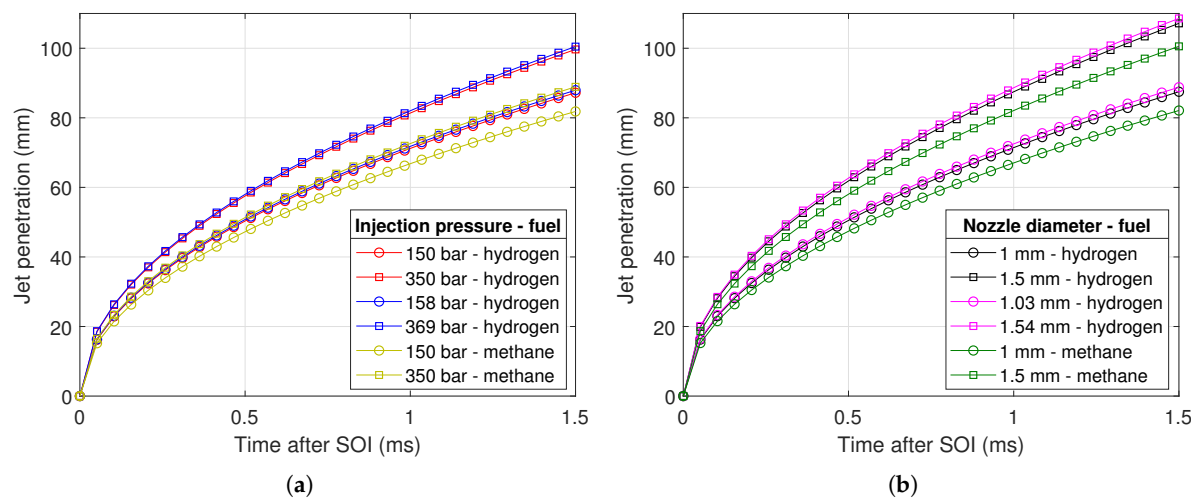

Figure 10. Jet tip penetration prediction for hydrogen and methane at (**a**) different injection pressures and 1 mm nozzle diameter and (**b**) different nozzle diameters and 150 bar injection pressure. The ambient density, pressure and temperature used in this model are 20.8 kg/m^3, 60 bar and 1000 K, respectively.

8.2. Fuel Delivery Strategies

Apart from the fuel injector, other parts of the on-board fuel delivery system also require further innovation. For instance, if the injection pressure were to be solely reliant on the storage pressure, the tank capacity can only be utilized until the instance when the storage pressure decreases below the set injection pressure. This would reduce the maximum achievable range of the vehicle. Integrating a hydrogen pump in the on-board fuel delivery system with a sufficiently small footprint could be a potential solution. A wide range of pneumatic-driven hydrogen booster pumps has recently been commercialized, with various output pressures as high as 1000 bar [115]. Despite the high cost of such a booster pump, it may still be a viable option to provide compressed hydrogen for research applications. However, a more cost-effective and robust tank-to-tip solution is required in the long run, before the hydrogen H2DDI technology can widely penetrate the transportation market.

9. Conclusions

This study reviews the current development of hydrogen internal combustion engines, with a focus on the hydrogen direct injection strategy. The port fuel injection engine configuration suffers many limitations, including pre-ignition, knocking, backfiring, low volumetric efficiency and compression loss problems. This limits the engine achievable load and efficiency. A potential solution to circumventing or alleviating these limitations is hydrogen direct injection. Despite being a promising strategy, the low engine compression ratio of typical SI engines limits the thermodynamic efficiency. In a compression-ignition engine, the spark ignition can be replaced by pilot fuel ignition, which induces multiple ignition kernels to promote fast combustion of gaseous fuel. This combustion mode, known as dual-fuel hydrogen-diesel direct injection, can potentially alleviate the power and compression ratio limitations reported for hydrogen applications in spark-ignition engines. When using green hydrogen, such combustion mode will greatly reduce the reliance on fossil fuels and thus reduce carbon-based emissions. However, hardware development for commercialization and research towards enhanced understanding of the mechanisms governing the engine efficiency and pollutant formation in such dual-fuel combustion mode is needed:

- Metal engine testing is required to prove the effectiveness of this combustion concept in terms of emissions and performance, and to investigate the effect of different operating parameters, for instance injector configuration and operation strategy.
- Fundamental optical and laser-based investigation as well as numerical simulations are needed to understand the governing mechanisms to facilitate engine performance optimization.
- For research purposes, this combustion mode can be studied by using single-fuel injectors—prototype injectors for hydrogen while using commercial diesel injectors to deliver pilot fuel. An integrated dual-fuel injector for hydrogen and pilot fuel may be needed as a long term solution.
- Further technological advancement towards a complete, compact, cost-efficient and robust on-board fuel delivery system is required for commercialization.

Abbreviations

ARENA	Australian Renewable & Energy Agency
BMEP	Brake mean effective pressure
BTDC	Before top dead center
BTE	Brake thermal efficiency
CA	Crank angle
CI	Compression ignition/compression ignited
CNG	Compressed natural gas
DI	Direct injection
EGR	Exhaust gas recirculation
FC	Fuel cell
GDI	Gasoline direct injection
HCCI	Homogeneous charge compression ignition
H2DDI	Hydrogen-diesel direct injection
HPDI	High pressure direct injection
ICE	Internal combustion engine
IMEP	Indicated mean effective pressure
ITE	Indicated thermal efficiency
MON	Motor Octane Number
NTSEL	National Traffic Safety & Environment Laboratory
PFI	Port fuel injection
RCEM	Rapid compression and expansion machine
RON	Research Octane Number
SI	Spark ignition/spark ignited
SOI	Start of injection

Nomenclature

A	Area
d	Diameter
D	Jet width
$\dot{m}_{max}$	Maximum mass flow rate
P	Pressure
R	Specific gas constant
s	Ratio of jet tip penetration to jet width
T	Temperature
t	Time after SOI
u	Velocity
Z	Jet tip penetration
ρ	Density
ϕ	Equivalence ratio
κ	Specific heat ratio

Subscripts

a	Ambient condition
o	Infinite fuel supply reservoir
eff	Effective
t	Time after SOI

Superscript

$*$	Sonic condition

References

1. Dong, X.; Wang, B.; Yip, H.L.; Chan, Q.N. CO_2 emission of electric and gasoline vehicles under various road conditions for China, Japan, Europe and world average—Prediction through year 2040. *Appl. Sci.* **2019**, *9*, 2295. [CrossRef]
2. Berry, G.D.; Pasternak, A.D.; Rambach, G.D.; Smith, J.R.; Schock, R.N. Hydrogen as a future transportation fuel. *Energy* **1996**, *21*, 289–303. [CrossRef]
3. Sharma, S.; Ghoshal, S.K. Hydrogen the future transportation fuel: From production to applications. *Renew. Sustain. Energy Rev.* **2015**, *43*, 1151–1158. [CrossRef]
4. Das, L.M. Hydrogen engines: A view of the past and a look into the future. *Int. J. Hydrogen Energy* **1990**, *15*, 425–443. [CrossRef]
5. Winkler-Goldstein, R.; Rastetter, A. Power to gas: The final breakthrough for the hydrogen economy? *Green* **2013**, *3*, 69–78. [CrossRef]
6. Abdalla, A.M.; Hossaina, S.; Nisfindy, O.B.; Azadd, A.T.; Dawoodb, M.; Azada, A.K. Hydrogen production, storage, transportation and key challenges with applications: A review. *Energy Convers. Manag.* **2018**, *165*, 602–627. [CrossRef]
7. *Hydrogen Scaling Up: A Sustainable Pathway for the Global Energy Transition*; Hydrogen Council: Belgium, 2017.
8. *Oil Market Report*; International Energy Agency: Paris, France, 2019.
9. The Observatory of Economic Complexity. Hydrogen Trade. Available online: https://atlas.media.mit.edu/en/profile/hs92/2804/ (accessed on 18 June 2019).
10. Bruce, S.; Temminghoff, M.; Hayward, J.; Schmidt, E.; Munnings, C.; Palfreyman, D.; Hartley, P. *National Hydrogen Roadmap: Pathways to an Economically Sustainable Industry*; The Commonwealth Scientific and Industrial Research Organization: Canberra, Australia, 2018.
11. Palmer, G. *Australia's Hydrogen Future*; Energy Transition Hub: Melbourne, Australia, 2018.
12. *Basic Hydrogen Strategy*; The Ministry of Economy, Trade and Industry: Tokyo, Japan, 2017.
13. Wegener, J. *Developments in Green Hydrogen Production and Use in Germany*; National Organization Hydrogen and Fuel Cell Technology: Berlin, Germany, 2019.

14. Banerjee, S.; Musa, M.N.; Jaafar, A.B. Economic assessment and prospect of hydrogen generated by OTEC as future fuel. *Int. J. Hydrogen Energy* **2017**, *42*, 26–37. [CrossRef]

15. Maggio, G.; Nicita, A.; Squadrito, G. How the hydrogen production from RES could change energy and fuel markets: A review of recent literature. *Int. J. Hydrogen Energy* **2019**, *44*, 11371–11384. [CrossRef]

16. Cornell, A. Hydrogen production by electrolysis. In Proceedings of the 1st International Conference on Electrolysis, Copenhagen, Denmark, 13–15 June 2017.

17. *Hydrogen Enabling a Zero Emission Europe: Technology Roadmaps Full Pack*; Hydrogen Europe: Brussels, Belgium, 2018.

18. *Hydrogen from Renewable Power: Technology Outlook for the Energy Transition*; International Renewable Energy Agency: Abu Dhabi, UAE, 2018.

19. *Opportunities for Australia from Hydrogen Exports*; ACIL Allen Consulting: Sydney, Australia, 2018.

20. *The Green Hydrogen Economy in the Northern Netherlands*; Noordelijke Innovation Board: Groningen, The Netherlands, 2017.

21. International Energy Agency. Hydrogen: A Key Part of a Clean and Secure Energy Future. Available online: https://www.iea.org/topics/hydrogen/demand/ (accessed on 19 October 2019).

22. Helmolt, R.V.; Eberle, U. Fuel cell vehicles: Status 2007. *J. Power Sources* **2007**, *165*, 833–843. [CrossRef]

23. Hänggi, S.; Elbert, P.; Bütler, T.; Cabalzar, U.; Teske, S.; Bach, C.; Onder, C. A review of synthetic fuels for passenger vehicles. *Energy Rep.* **2019**, *5*, 555–569. [CrossRef]

24. Manoharan, Y.; Hosseini, S.E.; Butler, B; Alzhahrani, H.; Senior, B.T.F; Ashuri, T; Krohn, J. Hydrogen fuel cell vehicles; Current status and future prospect. *Appl. Sci.* **2019**, *9*, 2296. [CrossRef]

25. Toyota and Kenworth unveil fuel cell heavy truck at Port of LA. *Fuel Cells Bull.* **2019**, *2019*, 3–4.

26. Verhelst, S. Recent progress in the use of hydrogen as a fuel for internal combustion engines. *Int. J. Hydrogen Energy* **2014**, *39*, 1071–1085. [CrossRef]

27. White, C.M.; Steeper, R.R.; Lutz, A.E. The hydrogen-fueled internal combustion engine: A technical review. *Int. J. Hydrogen Energy* **2006**, *31*, 1292–1305. [CrossRef]

28. *BMW Hydrogen Engine Reaches Top Level Efficiency*; BMW: Munich, Germany, 2009.

29. Ozcanli, M.; Bas, O.; Akar, M.A.; Yildizhan, S.; Serin, H. Recent studies on hydrogen usage in Wankel SI engine. *Int. J. Hydrogen Energy* **2018**, *43*, 18037–18045. [CrossRef]

30. Salazar, V.M.; Kaiser, S.A.; Halter, F. Optimizing precision and accuracy of quantitative PLIF of acetone as a Tracer for hydrogen fuel. *SAE Int. J. Fuels Lubr.* **2009**, *2*, 737–761. [CrossRef]

31. Kaiser, S.; White, C. PIV and PLIF to evaluate mixture formation in a direct-injection hydrogen-fuelled engine. *SAE Int. J. Engines* **2009**, *1*, 657–668. [CrossRef]

32. Wallner, T.; Scarcelli, R.; Nande, A.M.; Naber, J.D. Assessment of multiple injection strategies in a direct-injection hydrogen research engine. *SAE Int. J. Engines* **2009**, *2*, 1701–1709. [CrossRef]

33. Obermair, H.; Scarcelli, R.; Wallner, T. *Efficiency Improved Combustion System for Hydrogen Direct Injection Operation*; SAE Paper 2010-01-2170; SAE International: Warrendale, PA, USA, 2010. [CrossRef]

34. Scarcelli, R.; Wallner, T.; Salazar, V.M.; Kaiser, S.A. Modeling and experiments on mixture formation in a hydrogen direct-injection research engine. *SAE Int. J. Engines* **2010**, *2*, 530–541. [CrossRef]

35. Salazar, V.M.; Kaiser, S.A. An optical study of mixture preparation in a hydrogen-fueled engine with direct injection using different nozzle designs. *SAE Int. J. Engines* **2010**, *2*, 119–131. [CrossRef]

36. Scarcelli, R.; Wallner, T.; Matthias, N.; Salazar, V.; Kaiser, S. Mixture formation in direct injection hydrogen engines: CFD and optical analysis of single- and multi-hole nozzles. *SAE Int. J. Engines* **2011**, *2*, 2361–2375. [CrossRef]

37. Salazar, V.; Kaiser, S. *Interaction of Intake-Induced Flow and Injection Jet in a Direct-Injection Hydrogen-Fueled Engine Measured by PIV*; SAE Paper 2011-01-0673; SAE International: Warrendale, PA, USA, 2011. [CrossRef]

38. Matthias, N.S.; Wallner, T.; Scarcelli, R. A hydrogen direct injection engine concept that exceeds U.S. DOE light-duty efficiency targets. *SAE Int. J. Engines* **2012**, *5*, 838–849. [CrossRef]

39. Wallner, T.; Matthias, N.S.; Scarcelli, R.; Kwon, J.C. A Evaluation of the efficiency and the drive cycle emissions for a hydrogen direct-injection engine. *J. Automob. Eng.* **2013**, *227*, 99–109. [CrossRef]

40. Wimmer, A.; Wallner, T.; Ringler, J.; Gerbig, F. *H2-Direct Injection—A Highly Promising Combustion Concept*; SAE Paper 2005-01-0108; SAE International: Warrendale, PA, USA, 2005. [CrossRef]

41. Glaude, P.A.; Fournet, R.; Bounaceur, R.; Molière, M. Adiabatic flame temperature from biofuels and fossil fuels and derived effect on NO$_x$ emissions. *Fuel Process Technol.* **2010**, *91*, 229–235. [CrossRef]

42. Chong, C.T.; Hochgreb, S. Measurements of laminar flame speeds of liquid fuels: Jet-A1, diesel, palm methyl esters and blends using particle imaging velocimetry (PIV). *Proc. Combust. Inst.* **2011**, *33*, 979–986. [CrossRef]

43. Aleiferis, P.G.; Rosati, M.F. Controlled autoignition of hydrogen in a direct-injection optical engine. *Combust. Flame* **2012**, *159*, 2500–2515. [CrossRef]

44. Ingersoll, J.G. *Natural Gas Vehicles*; Fairmont Press: Lilburn, GA, USA, 1996.

45. Kondo, T.; Iio, S.; Hiruma, M. *A study on the Mechanism of Backfire in External Mixture Formation Hydrogen Engines—About Backfire Occurred by Cause of the Spark-Plug*; SAE Paper 971704; SAE International: Warrendale, PA, USA, 1997.

46. Lee, J.T.; Kim, Y.Y.; Lee, C.W.; Caton, J.A. An investigation of a cause of backfire and its control due to crevice volumes in a hydrogen fueled engine. *J. Eng. Gas Turbines Power* **2001**, *123*, 204–210. [CrossRef]

47. Huyskens, P.; Van Oost, S.; Goemaere, P.J.; Bertels, K.; Pecqueur, M. *The Technical Implementation of a Retrofit Hydrogen PFI System on a Passenger Car*; SAE Paper 2011-01-2004; SAE International: Warrendale, PA, USA, 2011. [CrossRef]

48. Zheng, J.; Liu, X.; Xu, P.; Liu, P.; Zhao, Y.; Yang, J. Development of high pressure gaseous hydrogen storage technologies. *Int. J. Hydrogen Energy* **2012**, *37*, 1048–1057. [CrossRef]

49. Antunes, J.G.; Mikalsen, R.; Roskilly, A.P. An investigation of hydrogen-fuelled HCCI engine performance and operation. *Int. J. Hydrogen Energy* **2008**, *33*, 5823–5828.

50. Caton, P.A.; Pruitt, J.T. Homogeneous charge compression ignition of hydrogen in a single-cylinder diesel engine. *Int. J. Engine Res.* **2009**, *10*, 45–63. [CrossRef]

51. Lee, K.J.; Kim, Y.R.; Byun, C.H.; Lee, J.T. Feasibility of compression ignition for hydrogen fueled engine with neat hydrogen-air pre-mixture by using high compression. *Int. J. Hydrogen Energy* **2013**, *38*, 255–264. [CrossRef]

52. Szwaja, S.; Grab-Rogalinski, K. Hydrogen combustion in a compression ignition diesel engine. *Int. J. Hydrogen Energy* **2009**, *34*, 4413–4421. [CrossRef]

53. Stenlåås, O.; Christensen, M.; Egnell, R.; Johansson, B.; Mauss, F. Hydrogen as homogeneous charge compression ignition engine fuel. *J. Fuels Lubr.* **2004**, *113*, 1317–1326.

54. Heffel, J.W. NO$_x$ emission and performance data for a hydrogen fueled internal combustion engine at 1500 rpm using exhaust gas recirculation. *Int. J. Hydrogen Energy* **2003**, *28*, 901–908. [CrossRef]

55. Heffel, J.W. NO$_x$ emission reduction in a hydrogen fueled internal combustion engine at 3000 rpm using exhaust gas recirculation. *Int. J. Hydrogen Energy* **2003**, *28*, 1285–1292. [CrossRef]

56. Mathur, H.B.; Das, L.M. Performance characteristics of a hydrogen fuelled S.I. engine using timed manifold injection. *Int. J. Hydrogen Energy* **1991**, *16*, 115–127. [CrossRef]

57. Lewis, B; von Elbe, G. *Combustion, Flames, and Explosions of Gases*; Academic Press: Orlando, FL, USA, 1987.

58. Tang, X.; Kabat, D.M.; Natkin, R.J.; Stockhausen, W.F.; Heffel, J. *Ford P2000 Hydrogen Engine Dynamometer Development*; SAE Paper 2002-01-0242; SAE International: Warrendale, PA, USA, 2002.

59. Stockhausen, W.F.; Natkin, R.J.; Kabat, D.M.; Reams, L.; Tang, X.; Hashemi, S.; Szwabowski, S.J.; Zanardelli, V.P. *Ford P2000 Hydrogen Engine Design and Vehicle Development Program*; SAE Paper 2002-01-0240; SAE International: Warrendale, PA, USA, 2002. [CrossRef]

60. Dimitriou, P.; Tsujimura, T. A review of hydrogen as a compression ignition engine fuel. *Int. J. Hydrogen Energy* **2017**, *42*, 24470–24486. [CrossRef]

61. Chintala, V.; Subramanian, K.A. A comprehensive review on utilization of hydrogen in a compression ignition engine under dual fuel mode. *Renew. Sustain. Energy Rev.* **2017**, *70*, 472–491. [CrossRef]

62. Santoso, W.B.; Bakar, R.A.; Nur, A. Combustion characteristics of diesel-hydrogen dual fuel engine at low load. *Energy Procedia* **2013**, *32*, 3–10. [CrossRef]

63. Sandalcı, T.; Karagöz, Y. Experimental investigation of the combustion characteristics, emissions and performance of hydrogen port fuel injection in a diesel engine. *Int. J. Hydrogen Energy* **2014**, *39*, 18480–18489. [CrossRef]

64. Saravanan, N.; Nagarajan, G. An experimental investigation of hydrogen-enriched air induction in a diesel engine system. *Int. J. Hydrogen Energy* **2008**, *33*, 1769–1775. [CrossRef]

65. Mohammadi, A.; Shioji, M.; Nakai, Y.; Ishikura, W.; Tabo, E. Performance and combustion characteristics of a direct injection SI hydrogen engine. *Int. J. Hydrogen Energy* **2007**, *32*, 296–304. [CrossRef]

66. Oikawa, M.; Ogasawara, Y.; Kondo, Y.; Sekine, K.; Takagi, Y.; Sato, Y. Optimization of hydrogen jet configuration by single hole nozzle and high speed laser shadowgraphy in high pressure direct injection hydrogen engines. *Int. J. Automot. Eng.* **2012**, *3*, 1–8.

67. Homan, H.S.; Reynolds, R.K.; De Boer, P.C.T; McLean, W.J. Hydrogen-fueled diesel engine without timed ignition. *Int. J. Hydrogen Energy* **1979**, *4*, 315–325. [CrossRef]

68. Furuhama, S.; Kobayashi, Y. Development of a hot-surface-ignition hydrogen injection two-stroke engine. *Int. J. Hydrogen Energy* **1984**, *9*, 205–213. [CrossRef]

69. Furuhama, S. Hydrogen engine systems for land vehicles. *Int. J. Hydrogen Energy* **1989**, *14*, 907–913. [CrossRef]

70. Welch, A.B.; Wallace, J.S. *Performance Characteristics of a Hydrogen-Fueled Diesel Engine with Ignition Assist*; SAE Paper 902070; SAE International: Warrendale, PA, USA, 1990. [CrossRef]

71. Wei, L. and Geng, P. A review on natural gas/diesel dual fuel combustion, emissions and performance. *Fuel Process. Technol.* **2016**, *142*, 264–278. [CrossRef]

72. Kawamura, A.; Sato, Y.; Naganuma, K.; Yamane, K.; Takagi, Y. *Development Project of a Multi-Cylinder DISI Hydrogen ICE System for Heavy Duty Vehicles*; SAE Paper 2010-01-2175; SAE International: Warrendale, PA, USA, 2010. [CrossRef]

73. Tanno, S.; Ito, Y.; Michikawauchi, R.; Nakamura, M.; Tomita, H. High-efficiency and low-NO_x hydrogen combustion by high pressure direct injection. *SAE Int. J. Engines* **2010**, *3*, 259–268. [CrossRef]

74. Takagi, Y.; Mori, H.; Mihara, Y.; Kawahara, N.; Tomita, E. Improvement of thermal efficiency and reduction of NO_x emissions by burning a controlled jet plume in high-pressure direct-injection hydrogen engines. *Int. J. Hydrogen Energy* **2017**, *42*, 26114–26122. [CrossRef]

75. Takagi, Y.; Oikawa, M.; Sato, R.; Kojiya, Y.; Mihara, Y. Near-zero emissions with high thermal efficiency realized by optimizing jet plume location relative to combustion chamber wall, jet geometry and injection timing in a direct-injection hydrogen engine. *Int. J. Hydrogen Energy* **2019**, *44*, 9456–9465. [CrossRef]

76. Kawamura, A.; Yanai, T.; Sato, Y.; Naganuma, K.; Yamane, K.; Takagi, Y. Summary and progress of the hydrogen ICE Truck development project. *SAE Int. J. Commer. Veh.* **2009**, *2*, 110–117. [CrossRef]

77. Naganuma, K.; Honda, T.; Yamane, K.; Takagi, Y.; Kawamura, A.; Yanai, T.; Sato, Y. Efficiency and emissions-optimized operating strategy of a high-pressure direct injection hydrogen engine for heavy-duty trucks. *SAE Int. J. Engines* **2010**, *2*, 132–140. [CrossRef]

78. Roy, M.K.; Kawahara, N.; Tomita, E.; Fujitani, T. High-pressure hydrogen jet and combustion characteristics in a direct-injection hydrogen engine. *SAE Int. J. Fuels Lubr.* **2012**, *5*, 1414–1425. [CrossRef]

79. Roy, M.K.; Kawahara, N.; Tomita, E.; Fujitani, T. Jet-guided combustion characteristics and local fuel concentration measurements in a hydrogen direct-injection spark-ignition engine. *Proc. Combust. Inst.* **2013**, *34*, 2977–2984. [CrossRef]

80. Verhelst, S.; Demuynck, J.; Sierens, R.; Scarcelli, R.; Matthias, N.S.; Wallner, T. *Update on the Progress of Hydrogen-Fueled Internal Combustion Engines*; Elsevier: Amsterdam, The Netherlands, 2013; pp. 381–400.

81. Trusca, B. High Pressure Direct Injection of Natural Gas and Hydrogen Fuel in a Diesel Engine. Master's Dissertation, The University of British Columbia, Vancouver, BC, Canada, 2000.

82. Hodgins, K.B.; Gunawan, H.; Hill, P.G. *Intensifier-Injector for Natural Gas Fueling of Diesel Engines*; SAE Paper 921553; SAE International: Warrendale, PA, USA, 1992. [CrossRef]

83. Miyake, M.; Biwa, T.; Endoh, Y.; Shimotsu, M.; Murakami, S.; Komoda, T. The development of high output, highly efficient gas burning diesel engines. In Proceedings of the CIMAC 1983, Paris, France, 1983.

84. Dai, L.M. Study of the Injection and Mixture Process and the Combustion Simulation of Natural Gas/Diesel Dual Fuel. Master's Dissertation, Jiangsu University, Zhenjiang, China, 2016.

85. Ishibashi, R; Tsuru, D. An optical investigation of combustion process of a direct high-pressure injection of natural gas. *J. Mar. Sci. Tech.* **2017**, *22*, 447–458. [CrossRef]

86. Douville, B. Performance, Emissions and Combustion Characteristics of Natural Gas Fueling of Diesel Engines. Master's Dissertation, The University of British Columbia, Kelowna, BC, Canada, 1994.

87. McTaggart-Cowan, G.; Mann, K.; Huang, J.; Singh, A.; Patychuk, B.; Zheng, Z.X.; Munshi, S. Direct injection of natural gas at up to 600 bar in a pilot-ignited heavy-duty engine. *SAE Int. J. Engines* **2015**, *8*, 981–996. [CrossRef]

88. White, T.R. Simultaneous Diesel and Natural Gas Injection for Dual-Fuelling Compression-Ignition Engines. Ph.D. Dissertation, University of New South Wales, Sydney, NSW, Australia, 2006.

89. Fink, G.; Jud, M.; Sattelmayer, T. Influence of the spatial and temporal interaction between diesel pilot and directly injected natural gas jet on ignition and combustion characteristics. *J. Eng. Gas Turb. Power.* **2018**, *140*, 102811. [CrossRef]

90. Fink, G.; Jud, M.; Sattelmayer, T. Fink. Fundamental study of diesel-piloted natural gas direct injection under different operating conditions. *J. Eng. Gas Turb. Power.* **2018**, *141*, 091006. [CrossRef]

91. Li, G.; Ouellette, P.; Dumitrescu, S.; Hill, P.G. Optimization study of pilot-ignited natural gas direct-injection in diesel engines. *SAE Int. J. Fuels Lubr.* **1999**, *108*, 1739–1748.

92. Yip, H.L.; Fattah, I.R.; Yuen, A.C.Y.; Yang, W.; Medwell, P.R.; Kook, S.; Yeoh, G.H.; Chan, Q.N. Flame-wall interaction effects on diesel post-injection combustion and soot formation processes. *Energy Fuels* **2019**, *33*, 7759–7769. [CrossRef]

93. Fattah, I.R.; Ming, C.; Chan, Q.N.; Wehrfritz, A.; Pham, P.X.; Yang, W.; Kook, S.; Medwell, P.R.; Yeoh, G.H.; Hawkes, E.R.; et al. Spray and combustion investigation of post injections under low-temperature combustion conditions with biodiesel. *Energy Fuels* **2018**, *32*, 8727–8742. [CrossRef]

94. Welch, A.; Mumford, D.; Munshi, S.; Holbery, J.; Boyer, B.; Younkins, M.; Jung, H. *Challenges in Developing Hydrogen Direct Injection Technology for Internal Combustion Engines*; SAE Paper 2008-01-2379; SAE International: Warrendale, PA, USA, 2008. [CrossRef]

95. McTaggart-Cowan, G.P.; Rogak, S.N.; Munshi, S.R.; Hill, P.G.; Bushe, W.K. Combustion in a heavy-duty direct-injection engine using hydrogen-methane blend fuels. *Int. J. Engine Res.* **2009**, *10*, 1–13. [CrossRef]

96. Australian Renewable Energy Agency. Enabling Efficient, Affordable & Robust Use of Renewable Hydrogen. Available online: https://arena.gov.au/projects/enabling-efficient-affordable-robust-renewable-hydrogen/ (accessed on 27 May 2019).

97. Naber, J.D.; Siebers, D.L. Hydrogen combustion under diesel engine conditions. *Int. J. Hydrogen Energy* **1998**, *23*, 363–371. [CrossRef]

98. Tsujimura, T.; Mikami, S.; Achiha, N.; Tokunaga, Y.; Senda, J.; Fujimoto, H. A study of direct injection diesel engine fueled with hydrogen. *SAE Int. J. Fuels Lubr.* **2003**, *112*, 390–405.

99. Turner, J.S. The 'starting plume' in neutral surroundings. *J. Fluid Mech.* **1962**, *13*, 356–368. [CrossRef]

100. Ouellette, P. Direct Injection of Natural Gas for Diesel Engine Fueling. Ph.D. Dissertation, University of British Columbia, Vancouver, BC, Canada, 1996.

101. Donaldson, C.D.; Snedeker, R.S. A study of free jet impingement. Part 1. Mean properties of free and impinging jets. *J. Fluid Mech.* **1971**, *45*, 281–319. [CrossRef]

102. Rogers, T. Mixture Preparation of Gaseous Fuels for Internal Combustion Engines Using Optical Diagnostics. Ph.D. Dissertation, RMIT University, Melbourne, Australia, 2014.

103. Chan, Q.N.; Fattah, I.R.; Zhai, G.; Yip, H.L.; Chen, T.B.Y.; Yuen, A.C.Y.; Yang, W.; Wehrfritz, A.; Dong, X.; Kook, S.; et al. Color-ratio pyrometry methods for flame-wall impingement study. *J. Energy Inst.* **2018**, *92*, 1968–1976. [CrossRef]

104. Fattah, I.M.R.; Yip, H.L.; Jiang, Z.; Yuen, A.C.Y.; Yang, W.; Medwell, P.R.; Kook, S.; Yeoh, G.H.; Chan, Q.N. Effects of flame-plane wall impingement on diesel combustion and soot processes. *Fuel* **2019**, *255*, 115726. [CrossRef]

105. Ouelette, P.; Goudie, D.; McTaggart-Cowan, G. Progress in the development of natural gas high pressure direct injection for Euro VI heavy-duty trucks. In *Internationaler Motorenkongress*; Springer: Berlin/Heidelberg, Germany, 2016; pp. 591–607.

106. Antunes, J.M.G.; Mikalsen, R.; Roskilly, A.P. An experimental study of a direct injection compression ignition hydrogen engine. *Int. J. Hydrogen Energy* **2009**, *34*, 6516–6522. [CrossRef]

107. Yamane, K.; Nogami, M.; Umemura, Y.; Oikawa, M.; Sato, Y.; Goto, Y. *Development of High Pressure H2 Gas Injectors, Capable of Injection at Large Injection Rate and High Response Using a Common-Rail Type Actuating System for a 4-Cylinder, 4.7-Liter Total Displacement, Spark Ignition Hydrogen Engine*; SAE Paper 2011-01-2005; SAE International: Warrendale, PA, USA, 2011. [CrossRef]

108. Baert, R.; Klaassen, A.; Doosje, E. Direct injection of high pressure gas: Scaling properties of pulsed turbulent jets. *SAE Int. J. Engines* **2010**, *3*, 383–395. [CrossRef]

109. Bovo, M.; Rojo, B. *Single Pulse Jet Impingement on Inclined Surface, Heat Transfer and Flow Field*; SAE Paper 2013-24-0003; SAE International: Warrendale, PA, USA, 2013. [CrossRef]

110. Hill, P.G.; Ouellette, P. Transient turbulent gaseous fuel jets for diesel engines. *J. Fluid Eng.* **1999**, *121*, 93–101. [CrossRef]

111. Hajialimohammadi, A.; Edgington-Mitchell, D.; Honnery, D.; Montazerin, N.; Abdullah, A.; Mirsalim, M.A. Ultra high speed investigation of gaseous jet injected by a single-hole injector and proposing of an analytical method for pressure loss prediction during transient injection. *Fuel* **2016**, *184*, 100–109. [CrossRef]

112. Rubas, P.J. An Experimental Investigation of the Injection Process in a Direct-Injected Natural Gas Engine Using PLIF and CARS. Ph.D. Dissertation, University of Illinois at Urbana-Champaign, Champaign, IL, USA, 1998.

113. Yu, J.; Vuorinen, V.; Hillamo, H.; Sarjovaara, T.; Kaario, O.; Larmi, M. *An Experimental Study on High Pressure PULSED jets for DI Gas Engine Using Planar Laser-Induced Fluorescence*; SAE Paper 2012-01-1655; SAE International: Warrendale, PA, USA, 2012. [CrossRef]

114. Hamzehloo, A.; Aleiferis, P.G. Large eddy simulation of highly turbulent under-expanded hydrogen and methane jets for gaseous-fuelled internal combustion engines. *Int. J. Hydrogen Energy* **2014**, *39*, 21275–21296. [CrossRef]

115. Haskel. Hydrogen. Available online: https://www.haskel.com/industries/hydrogen/ (accessed on 25 June 2019).